Estimating continental river basin discharges using multiple remote sensing data sets

Arthur W. Sichangi [a,c], Lei Wang [a,b,*], Kun Yang [a,b], Deliang Chen [d], Zhongjing Wang [e,f], Xiuping Li [a], Jing Zhou [a], Wenbin Liu [a], David Kuria [g]

[a] *Key Laboratory of Tibetan Environment Changes and Land Surface Processes, Institute of Tibetan Plateau Research, Chinese Academy of Sciences, Beijing, China*
[b] *CAS Center for Excellence in Tibetan Plateau Earth Sciences, Beijing, China*
[c] *University of Chinese Academy of Sciences, Beijing, China*
[d] *Department of Earth Sciences, University of Gothenburg, Gothenburg, Sweden*
[e] *State Key Laboratory of Hydroscience and Engineering, Tsinghua University, Beijing*
[f] *Department of Hydraulic Engineering, Tsinghua University, Beijing*
[g] *Dedan Kimathi University of Technology, Nyeri, Kenya*

ARTICLE INFO

ABSTRACT

Rivers act as a source of fresh water for terrestrial life, yet the discharges are poorly documented since the existing direct observations are inadequate and some observation stations have been interrupted or discontinued. Discharge estimates using remote sensing thus have a great potential to supplement ground observations. There are remote sensing methods established to estimate discharge based on single parameter derived relationships; however, they are limited to specific sections due to their empirical nature. In this study, we propose an innovative method to estimate daily discharges for continental rivers (with river channel widths >800 m (Birkett and Beckley, 2010)) using two satellite derived parameters. Multiple satellite altimetry data and Moderate Resolution Imaging Spectroradiometer (MODIS) data are used to provide a time series of river stages and effective river width. The derived MODIS and altimetry data are then used to optimize unknown parameters in a modified Manning's equation. In situ measurements are used to derive rating curves and to provide assessments of the estimated results. The Nash–Sutcliffe efficiency values for the estimates are between 0.60 and 0.97, indicating the power of the method and accuracy of the estimations. A comparison with a previously developed empirical multivariate equation for estimating river discharge shows that our method produces superior results, especially for large rivers. Furthermore, we found that discharge estimates using both effective river width and stage information consistently outperform those that only use stage data.

1. Introduction

River discharge measurements are essential for flood management, climate studies, and water resources management. Knowledge of river flow propagation speed, i.e., the time for flows to pass downstream, is critical for watershed modeling, flood prediction, and managing reservoirs (Brakenridge et al., 2012). Therefore, there is a great need for long-term, continuous, spatially consistent, and readily available discharge data.

River discharges are currently recorded at river gauging stations. However, the availability of gauging station records is generally decreasing in most parts of the world, with data for some areas either

completely unavailable or difficult to access for timely use in operational flood forecasting and disaster prevention (Dai & Trenberth, 2002; Dai, Qian, Trenberth, & Milliman, 2009). Tourian, Sneeuw, and Bárdossy (2013) compiled a time series plot of the number of stations with available discharge data from the publicly available data of the Global Runoff Data Centre (GRDC). This time series indicates a decline in the total monitored annual stream flows between 1970 and 2010. Inadequate discharge observation has become a major problem in both developing and underdeveloped countries, as a majority of stations are no longer in operation (Calmant & Seyler, 2006). Similarly, the commitments of participating countries to initiatives such as the International Hydrological Decade (1965–1974), which was the basis for the assessment of water resources conditions worldwide, have been seriously decreasing (Vörösmarty et al., 2001). In addition to the decrease in the number of stations that contribute to the Global Runoff Database, some stations have discontinuous datasets. These data gaps present a challenge for

making useful analyzes. Furthermore, current data collection efforts are mainly focused on individual development projects in different countries. This trend has produced a patchwork of datasets that span short periods of time, with restricted spatial coverage and limited availability.

Satellite altimetry, whose application over land has increased in recent decades, is an interesting alternative for recording periodic variations in water level in continental environments with acceptable accuracy. It appears to be a highly promising source of information that may be used to complement ground station data. The ability of satellite altimeters to monitor continental water surfaces and to measure their stage has been demonstrated for continental waters (Calmant & Seyler, 2006; Jarihani, Callow, Johansen, & Gouweleeuw, 2013; Koblinsky, Clarke, Brenner, & Frey, 1993; Sulistioadi et al., 2015), and this method has been used to provide estimates of river discharge (Sneeuw et al., 2014). Recent studies demonstrate a growing interest in deriving discharge estimates from remote sensing via spectral bands (Brakenridge, Nghiem, Anderson, & Mic, 2007; Temimi et al., 2011) and altimeters (Leon et al., 2006). In addition to discharge estimation, attempts to use remote sensing data (river width or water surface elevation) as surrogates for in situ measurements in hydrological model calibration have also been tested (Sun, Ishidaira, & Bastola, 2012a,b). A fundamental requirement for estimating river discharge lies in the ability to realistically estimate spatial hydraulic variables, e.g., river width and water surface heights, and to establish a relationship between interrelated hydraulic variables that can then be used to estimate other variables such as depth (Mersel, Smith, Andreadis, & Durand, 2013).

Traditionally, the hydraulic characteristics of stream channels including depth (d), width (w), and velocity (v) are measured quantitatively at a ground observation stations, and these parameters vary with discharge as simple power functions at a given river cross-section. Consequently, the structure primarily used for river discharge measurements is the channel cross-section. The total instantaneous water flux (Q), in m^3/s or ft^3/s, through the cross-section is equal to the product of the mean cross-sectional flow as in Eq. (1), as averaged from numerous ground station measurements taken across the stream (Smith & Pavelsky, 2008).

$$Q = w \times d \times v. \tag{1}$$

According to Leopold and Maddock (1953), the functions derived for a given cross-section and among various cross-sections along the river only differ in the numerical values of the coefficients and exponents in accordance with Eqs. (2), (3), and (4).

$$w = aQ^b \tag{2}$$

$$d = cQ^f \tag{3}$$

$$v = kQ^m \tag{4}$$

where a, b, c, f, k, and m are empirical constants.

Since the estimates of river discharge require the utilization of w, d, and v, any attempts to neglect one of the parameters contributes to increased errors. For instance, Bjerklie, Moller, Smith, and Dingman (2005) estimated in-bank river discharge using remotely sensed width information and channel slope but acknowledged that this model is a less accurate method compared to discharge estimation models that include width, depth, and slope (Bjerklie, Lawrence Dingman, Vorosmarty, Bolster, & Congalton, 2003). Most discharge estimation methods use regression based relationships between remotely measured parameters (e.g., w or stage) and in situ measured discharge via the stated equations (Smith & Pavelsky, 2008; Tarpanelli, Barbetta, Brocca, & Moramarco, 2013). Unfortunately, this approach is not suitable for all river environments (LeFavour & Alsdorf, 2005). For some river sections, e.g., a rectangular cross-section, changes in water height yields negligible changes in the width but significant changes in the

flow. This precludes the use of a w-based estimation equation (Sun et al., 2012b). The reverse is true in flat terrains/river sections where changes in river width yield negligible changes in river heights, e.g., the Diamantina River in Central Australia (Jarihani, Callow, McVicar, Van Niel and Larsen, 2015; Jarihani, Larsen, Callow, McVicar and Johansen, 2015). This rules out the use of an estimation equation based on d.

Consequently, utilizing the river stage level from satellite altimetry data in conjunction with other space-based parameters, e.g., river width and river surface velocity from Synthetic Aperture Radar (SAR) (Bjerklie et al., 2005), should generate estimates of discharge that are superior to those based on a single parameter.

Several researchers have reviewed the types of river hydraulic information that can potentially be observed from space-based platforms and have produced several general relationships that utilize this information for the development of a wide range of river discharge estimation equations (Alsdorf, Rodríguez, & Lettenmaier, 2007; Bjerklie et al., 2003; Tang, Gao, Lu, & Lettenmaier, 2009). In all cases, the success of discharge estimation using remote sensing derived parameters depends on the accuracy of estimate parameters, e.g., width and stage, and the ability to accurately derive the parameters that cannot be directly observed from space, e.g., velocity and bathymetry depth. Since these initial studies, various approaches have been used to estimate discharge by considering a wide range of strategies to improve outcomes (Table 1).

On the basis of the previous studies listed in Table 1, four approaches to estimating river discharge using remote sensing can be summarized as follows:

a) Measure water level variation using satellite altimetry data. These measurements are then converted to river discharge on the basis of a rating curve between satellite-derived "water level" and in situ measured discharge.

b) Correlate satellite derived water surface area with in situ measured discharge, and then infer river discharge from satellite data on the basis of the water area–discharge rating curve.

c) Using hydraulic equations, estimate river discharge from the measurement of hydraulic variables from satellite and/or other remotely obtained information.

d) Using remotely sensed data, i.e., river flow widths, to approximate the newly discovered characteristic scaling law that has been termed at-many-stations hydraulic geometry (AMHG). AMHG halves the number of parameters required by traditional hydraulic geometry, thus paving the way for discharge estimation solely from remote sensing (Gleason & Smith, 2014).

The first approach uses satellite altimetry data (Birkinshaw et al., 2010; Tarpanelli et al., 2013). The second approach relies on changes in river width (Pavelsky, 2014; Smith & Pavelsky, 2008). The third approach has been invoked by several researchers (Bjerklie et al., 2005; Bjerklie et al., 2003; LeFavour & Alsdorf, 2005; Negrel, Kosuth, & Bercher, 2011). The last approach marks a breakthrough in discharge estimation using remote sensing without requiring any in situ measurements or a priori information. Gleason, Smith, and Lee (2014) advanced the AMHG discharge retrieval approach via additional parameter optimizations and the study performed a validation for 34 gauged rivers that span a diverse range of geomorphic and climatic settings. This study reported successful retrieval in channel discharges for a variety of rivers. However, there were exceptions which include braided rivers, low-b rivers (i.e., having a mean cross-sectional at station hydraulic geometry b value <0.1), and rivers displaying extreme variability in discharge as manifested in the tested arid-climate rivers. To address these exceptions, further studies are required that incorporate the currently used river width AMHG with the at-station hydraulic geometry Eqs. (2) and (3). An approach that could estimate river discharge solely from remotely obtained hydraulic data, i.e., width, depth and velocity,

would be most attractive. To date, few such studies have been reported, owing to the restrictions of current sensors. For example, the average velocity cannot be directly measured from satellite or other remote data sources at present. In addition, limitations in the measurement of slope have also been reported. For instance, Birkinshaw et al. (2014) estimated discharge at three locations on the Mekong and Ob Rivers by using an equation from Bjerklie et al. (2003) that was developed from a database of 1012 discharge measurement ranging in magnitude from <1 m³/s to over 200,000 m³/s. Slope is an important parameter in Manning's equation (Manning, 1889). However, Birkinshaw et al. (2014) estimated slope using measurements derived from the satellite altimetry traverse for the location where the discharge was to be estimated and the next downstream altimetry crossing site. This slope estimation method assumes that the water surface variation at the two sites is similar, which at times may produce inaccurate results. In addition, the availability of another virtual station (i.e., the point of intersection between the satellite tracks with the river) at a desired distance is always not guaranteed. LeFavour and Alsdorf (2005) used the channel depths averaged from nautical charts which is only possible for navigable rivers. Bjerklie et al. (2005) found that incorporation of velocity from SAR substantially improves the accuracy of river discharge estimate. However, this approach is limited by the availability of surface velocity data which is collected on an infrequent basis depending on the orbits of satellites.

Table 1
Overview of studies using remote sensing to estimate river discharge (the current paper is added for completeness). Not all studies have performed river discharge estimation by incorporating multiple remote sensing derived datasets. In addition, not all studies have compared the accuracies in considering the single verses the multiple derived remote sensing data. Not all models used in the studies are optimized for diverse river cross-sections. In this case, the three are flagged as not applicable (N/A) in the key results. In the 'Key results' column the abovementioned three components are identified by the code: (1) use of multiple remote sensing derived dataset, (2) comparison in discharge estimate using single verses multiple derived remote sensing data and (3) performance over diverse river cross-sections.

Study	Data used	Approach	Key results
Gleason and Smith (2014)	Landsat TM	Landsat TM are used to approximate at-many-stations (AMHG). AMHG used to retrieve instantaneous river discharge.	1. N/A 2. N/A 3. AMHG discharge retrievals are successful for most investigated river morphologies. However, poor performance is observed in a few rivers (Gleason et al., 2014).
Birkinshaw et al. (2014)	ERS 2, Envisat & Landsat	The satellite data are applied to the Bjerklie et al. (2003) equation.	1. Multiple parameters (width, slope, stage) 2. N/A 3. Nash–Sutcliffe efficiency values of 0.90 at Nakhon Phanom and 0.86 at Vientiane on the Mekong, and 0.86 at Kalpashevo on the Ob
Pavelsky (2014)	Rapid Eye & Landsat	Width based rating curves are used.	1. N/A 2. N/A 3. Optimized to use width and tested on river Tanana with a 6.7% relative error
Tarpanelli et al. (2013)	ERS 2 & ENVISAT	Rating Curve Model is applied to estimated discharge using altimetry data. Comparison of the method is carried out against the empirical equation proposed by Bjerklie et al. (2003).	1. N/A 2. N/A 3. Optimized to use stage and tested on Po River with a relative root mean square error of 30%
Negrel et al. (2011)	Acoustic Doppler Current Profiler (ADCP)	The hydraulic parameters values are formulated using least square method by minimization of the error criterion.	1. No remote sensing data was used to test this method. Instead datasets were taken at gauging stations in the Amazon basin. 2. N/A 3. Two sites Obidos and Manacupuru are considered with the former recording poor performance.
Birkinshaw et al. (2010)	ERS-2 and ENVISAT	Stage based rating curves are used	1. N/A 2. N/A 3. Optimized to use stage giving Nash–Sutcliffe values between 0.823 and 0.935 on River Mekong
Smith and Pavelsky (2008)	MODIS	Width based rating curves are used	1. N/A 2. N/A 3. Optimized to use river width giving a mean absolute error <25% on River Lena
LeFavour and Alsdorf (2005)	SRTM DEM, SAR, nautical charts	Manning's equation is used with SRTM DEM slope and with channel width measurements from the SAR, channel depths averaged from nautical charts, and reasonable estimates of Manning's n.	1. Remotely sensed parameters width and slope are used 2. N/A 3. Three sites are considered giving discharge values within 6.2% at Manacupuru, 7.6% at Itapeua, and 0.3% at Tupe of the in situ gage-based estimates.
Bjerklie et al. (2005)	Topographical maps aerial photos, SAR	Hydraulic relationship is used to estimate in-bank river discharge using remotely sensed data (Bjerklie et al., 2003).	1. Remote sensing derived slope, velocity and width are used 2. N/A 3. Attained mean discharge estimate accuracy within 10% over River Missouri.
Bjerklie et al. (2003)		Multiple regression analysis used to develop multi-variate river discharge estimating equations is developed.	1. Different combinations of remote sensing derived effective river width, stage and surface velocity of river estimates discharge with average uncertainty of <20%. 2. N/A 3. N/A
This study	MODIS & Multiple Satellite altimetry	River stage is incorporated with the effective river width. A comparison is done against a stage derived discharge estimation equation and the empirical equation proposed by (Bjerklie et al., 2003).	1. Satellite derived river stage and effective river width are used. 2. A comparison is drawn showing a better performance. 3. We formulate our model to capture variations in river cross sections. Good performance is exhibited in the tested cross sections.

Table 2
A summary of the study rivers describing the upstream basin size, satellite altimeter used followed by the satellite track in brackets, upstream length, an averaged discharge for the study period (2003 − 2010), the locations of the in situ station (Lat, Lon) and the distance (*dis*) of the virtual station from the in situ station.

Site	Basin (km²)	Satellite altimeter	Length (km)	Discharge (m³/s)	Lat (°)	Lon (°)	*Dis* (km)
Mississippi	2,964,255	Envisat	1690	21,415	32.31	− 90.91	4
Yangtze	1,705,383	Envisat (894), Jason-2 (164)	4258	26,620	30.77	117.62	106
Congo	3,475,000	Envisat (014), Jason-2 (248)	2986	40,131	− 4.30	15.30	292
Danube	131,331	Envisat	1179	1945	47.82	18.77	150
Volga	1,360,000	Envisat	2847	7787	48.48	45.20	94
Yenisey	2,440,000	Envisat	2698	20,121	67.26	86.55	22
Lena	2,430,000	Envisat	3339	18,882	70.66	127.24	20
Amazon, Jatuanara	2,854,286	Envisat (063 & 607), Jason-2 (152)	4792	128,826	− 3.14	− 59.46	106
Amazon, Manacupuru	2,147,736	Envisat (0149), Jason-2 (063)	4690	110,234	− 3.35	− 60.22	80
Sao Paulo De Olivenca	990,781	Envisat (121 & 078), Jason-2 (089)	2883	48,344	− 3.41	− 68.86	201
Santo Antonio Do Ica	1,134,540	Envisat (035), Jason-2 (178)	3084	57,984	− 3.09	− 67.94	154
Sao Felipe	110,862	Envisat (493), Jason-2 (089)	639	8610	0.37	− 67.31	1
Canutama	230,012	Envisat (736, 278 & 407), Jason-2 (254)	1181	6204	− 6.52	− 64.52	18
Rio Negro Serrinha	279,945	Envisat (364, 407 & 865), Jason-2 (165)	1160	18,589	− 0.37	− 64.45	1

Our methodology is an improvement on the tabulated methods (Table 1) in the following ways. First, our method applies to a wide range of channels, i.e., rectangular, arc, and trapezoidal, which are widely perceived to be the major ideal river section. Secondly, we use stage and effective river width to optimize all the unknown parameters whose direct measurement from space is limited, e.g., estimation of slope using satellite altimetry (Birkinshaw et al., 2014). Finally, we show that with the increasing number of satellite altimetry missions, this discharge estimation holds promise.

The overarching aim of this research is to extend the previous studies by using both the effective river width and stage to optimize the unknown parameters in a discharge rating equation. Therefore, the main objectives in this study are:

(a) Comparing discharge in two cases: (i) discharge estimation using just stage data; and (ii) discharge estimation using stage and effective river width, i.e., Model 1.

(b) Comparing two methods; Model 1 and a previously existing equation, i.e., Model 2 which requires the estimation of effective river width, depth and slope.

2. Materials and pre-processing

2.1. Major rivers and ground observations

We used data from eight of the world's major rivers, namely, the Mississippi (Vicksburg MS Station), the Yangtze (Datong Station), the Congo (Kinshasa Station), the Danube (Bratislava Station), the Volga (Volgograd Power Plant), the Amazon and its tributaries (Jatuanara, Manacupuru, Sao Paulo De Olivenca, Santo Antonio Do Ica, Sao Felipe, Canutama, and Serrinha Stations), the Lena (Kyusyur), and the Yenisey (Igarka). Detailed characteristics of the rivers are presented in Table 2.
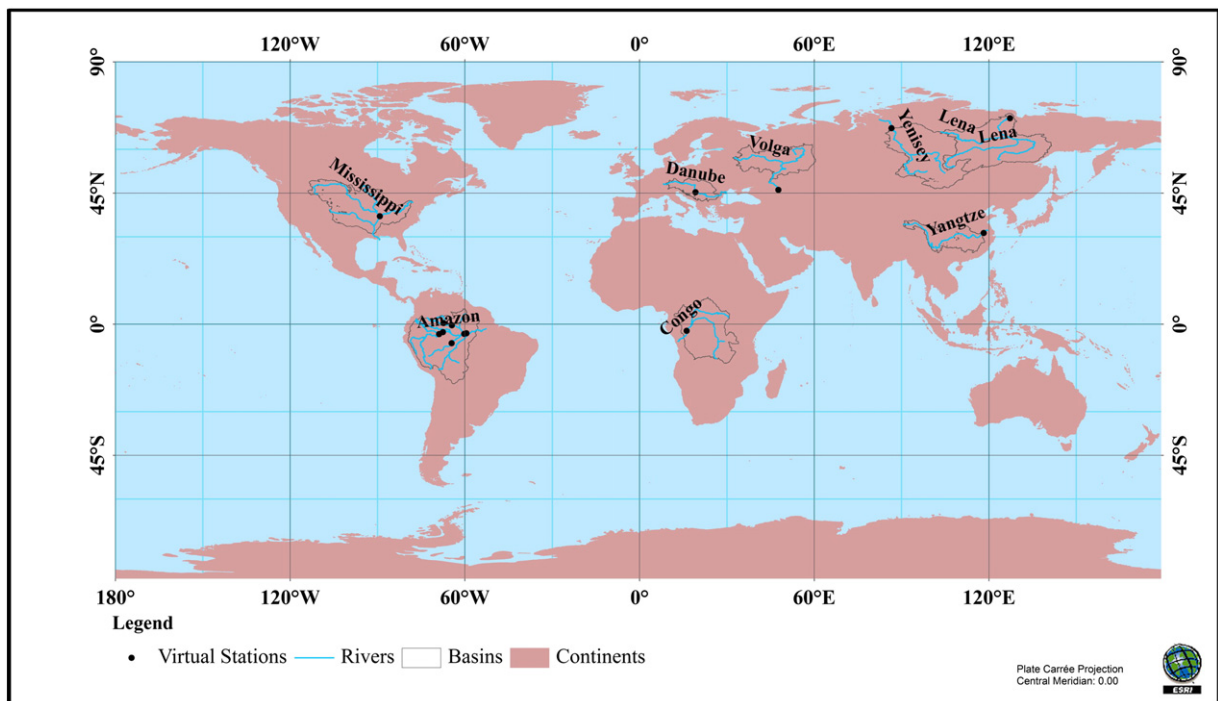

Fig. 1. The spatial distribution of the rivers studied.

Table 3
Estimated slope and related errors.

River/station	Slope (cm/km)
Amazon (Jatuanara)	1.8 ± 0.17
Purus (Canutama)	7.4 ± 0.71
Amazon (Manacupuru)	1.4 ± 0.12
Negro (Sao Felipe)	5.4 ± 0.61
Amazon (Santo Antonio Do Ica)	2.4 ± 0.21
Amazon (Sao Paulo De Olivencia)	3.4 ± 0.32
Negro (Serrinha)	6.9 ± 0.59

Various sections of all the targeted rivers have been traversed by satellite altimetry (Fig. 1).

2.2. Satellite observations

2.2.1. Altimetry data

Radar altimetry consists of vertical range measurements between the satellite and the surface. The altimeter satellite is placed on a repeat orbit and flies over a given region at regular time intervals (termed the orbital cycle). The altimeter emits a radar pulse and measures the two-way travel time from the satellite to the surface. The altimeter range (R) is therefore derived with a precision of a few centimeters. For instance, a case studies by Jarihani et al. (2013) and Santos da Silva et al. (2010) gave precision values of 0.12–0.40 m for Envisat, 1.07 m for Jason-1, and 0.96 m for Topex. However, precision can vary widely depending on the surface characteristics, for instance, the topography and surrounding vegetation. The satellite altitude (h) with respect to the reference ellipsoid is precisely known from orbit modeling. Altimeter measurements of surface topography are distorted, and therefore corrections are applied ($\sum e$). For example, atmospheric propagation effects in the troposphere and the ionosphere, electromagnetic bias, residual geoid errors, and inverse barometer effects can all distort

measurements (Santos da Silva et al., 2010; Shum, Ries, & Tapley, 1995). Taking into account propagation delays from the interactions of electromagnetic waves in the atmosphere and geophysical corrections, the height of the reflecting surface (H) with respect to a reference ellipsoid can be estimated using Eq. (5) below:

$$H = h - R - \sum e. \tag{5}$$

In this study, we use altimetry data whose listed corrections have been applied. Currently, the altimeter missions in operation include Saral, HY-2, Cryosat, and Jason-2. Past missions include ERS-1 (1991–2000), Topex/Poseidon (1992–2006), ERS-2 (1995–2011), GEOSAT Follow-On (GFO) (1998–2008), Jason-1 (2001–2005), and Envisat (2002−2012) (Jarihani et al., 2013). ERS-1, ERS-2, and Envisat have a 35-day temporal resolution (duration of the orbital cycle) and an inter-track spacing of approximately 85 km at the equator. Topex, Jason-1, and Jason-2 have a 10-day orbital cycle and an equatorial inter-track spacing of 350 km. GFO has a 17-day orbital cycle and an equatorial inter-track spacing of 170 km. GFO exhibits relatively large errors in water elevation estimations compared to Envisat and Jason-2 derived elevation data (Jarihani et al., 2013). Envisat is considered as an improvement on ERS-2 altimetry as proven by the accuracy of the water level retrievals (Santos da Silva et al., 2010). The combined global altimetry dataset covers more than two decades, and it will be continuously updated in the coming decades (Crétaux et al., 2011). Combining altimetry data from several altimetry missions increases the temporal resolution as well as the length of the time series. For instance, Schwatke, Dettmering, Bosch, and Seitz (2015) developed a method that is based on an extended outlier rejection and a Kalman filter approach that incorporates cross-calibrated multi-mission altimeter data from Envisat, ERS-2, Jason-1, Jason-2, TOPEX/Poseidon, and SARAL/AltiKa. However, prior to Kalman filtering various user-
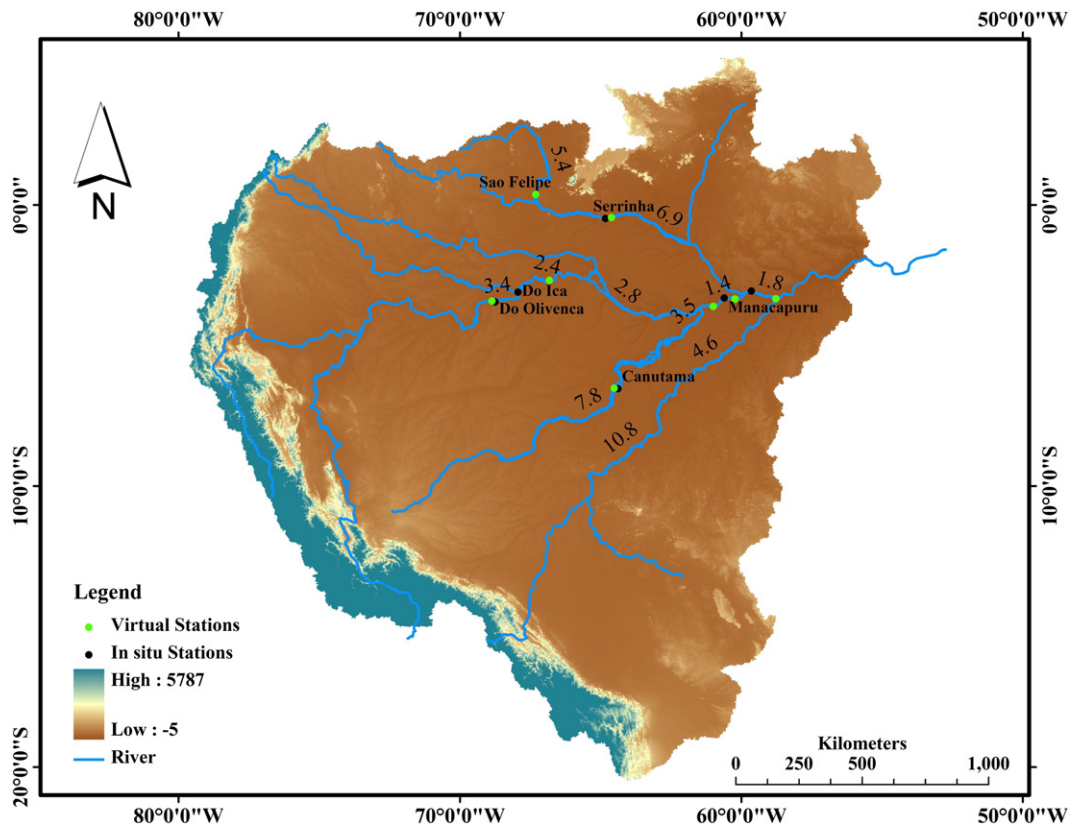

Fig. 2. The Amazon River Basin. The numbers on the figure represent the river slope in cm/km derived from DEM in each river segment. The errors associated with the slopes were determined by adjusting the line of best fit by the fit error. The resultant slopes and their respective error are given in Table 3.
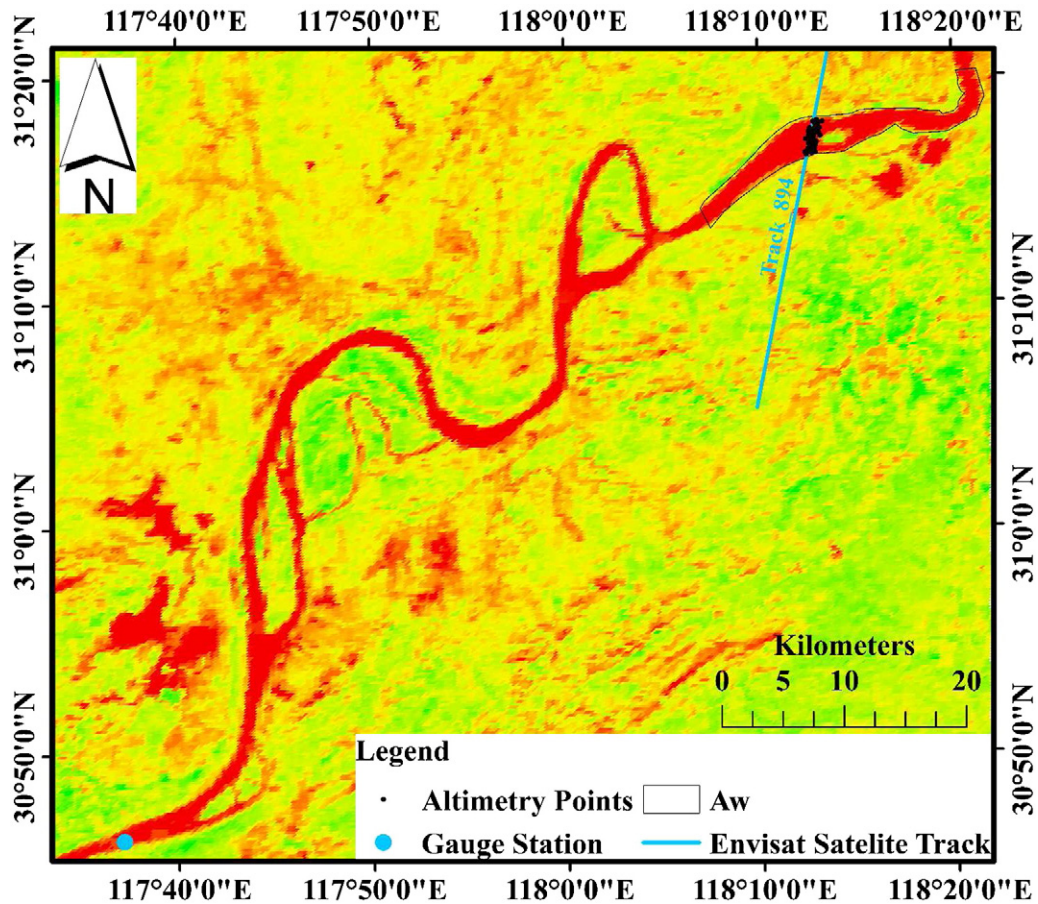
Fig. 3. An example of overlapped Band 2 of MODIS (acquired on 14 Jan 2003) and altimetry passes at the virtual station of Yangtze (near Datong Station). The satellite images were used in obtaining the water surface area (A_w), whereas the multiple altimetry data was used to obtain stage data.

defined outlier rejections must be applied to eliminate inaccurate water levels. This limits the applicability of the method to a restricted number of river locations whose altimetry missions meet the predefined criteria.

According to Birkinshaw et al. (2010), the measurement of stage at two points with some distance apart, in their case 400 km, is reasonably sufficient to estimate the discharge of most large rivers. In their study, a direct comparison is carried out without loss of generality. This prompted us to investigate the possibility of a multiple satellite altimetry dataset (Envisat and Jason-2 in Table 2) by considering the closest satellite observations to the in situ stations. We defined a selection criterion based on the condition that the virtual stations were located between tributaries or outflows. With this condition, a total of 9 sites had multiple satellite altimetry dataset within the defined reach (Table 2). Some river reaches had more than one Envisat virtual station, for instance, locations near the Amazon's Canutama, Serrinha, Sao Paulo De Olivenca and Jatuanara stations (Table 2). However, in other reaches the Envisat data from a single station was the only data, e.g., near the Mississippi (Vicksburg MS station), Danube (Bratislava Volgograd power plant station), Yenisey (Igarka station), and Lena (Kyusyur station) as shown in Table 2. The satellite data were then adjusted to a common datum, GGM02C. Jason-2 datasets were corrected for height difference with the Envisat dataset. This was done by computing the average height difference between the two sets of virtual stations. The two datasets were then merged.

Envisat provides data from 2002 to 2010 with a change of orbit in the remaining two years that coincides with other datasets such as MODIS (2000–present) and the in situ measurements from GRDC (whose start and end periods differ but covers the study period of 2002–2009). It also provides an extended data for the period which Jason-2 wasn't available i.e. before 2008. This longer epoch of Envisat meets the aims of our study. It was designed to serve as a successor to the ERS-1 and ERS-2 satellites of the European Space Agency. It carries 10 complementary instruments, including a radar altimeter (RA). The radar altimeter is a nadir-pointing and operates at two frequencies: Ku-band (13.575 GHz/wavelength, 2.3 cm) and S-band (3.2 GHz/ 9.3 cm) (Zelli & Aerospazio, 1999). The along-track resolution of the Envisat RA-2 is approximately 350 m in high frequency mode with a footprint of ~1.7 km in diameter (Sulistioadi et al., 2015). Envisat provides observations along its entire ground track over the ocean and continental surfaces, which extends from 82.4° N to 82.4° S with an equatorial ground track spacing of approximately 85 km (Leon et al., 2006).

On the other hand, the incorporation of Jason-2 is advantageous in the three ways. First, it has a higher temporal resolution (10 days) and therefore increases the discharge estimate days. Second, Jason-2 is still operational and therefore ensures continuity in discharge estimation. Finally, the PISTACH algorithm in Jason-2 provides more accurate altimetry data compared to other sources (Jarihani et al., 2013). Jason-2 was launched in mid-2008 as the Jason-1 follow-up mission, and it has since acquired data over inland water bodies. Jason-2 carries a high-precision radar altimeter operating in Ku band (13.6 GHz) and C band (5.3 GHz) with a footprint of ~2–4 km in diameter depending on surface roughness (Fabrice Papa et al., 2012).

The Envisat and Jason-2 altimetry datasets for all the rivers under study were provided by two databases: the *Laboratoired' Etudesen*
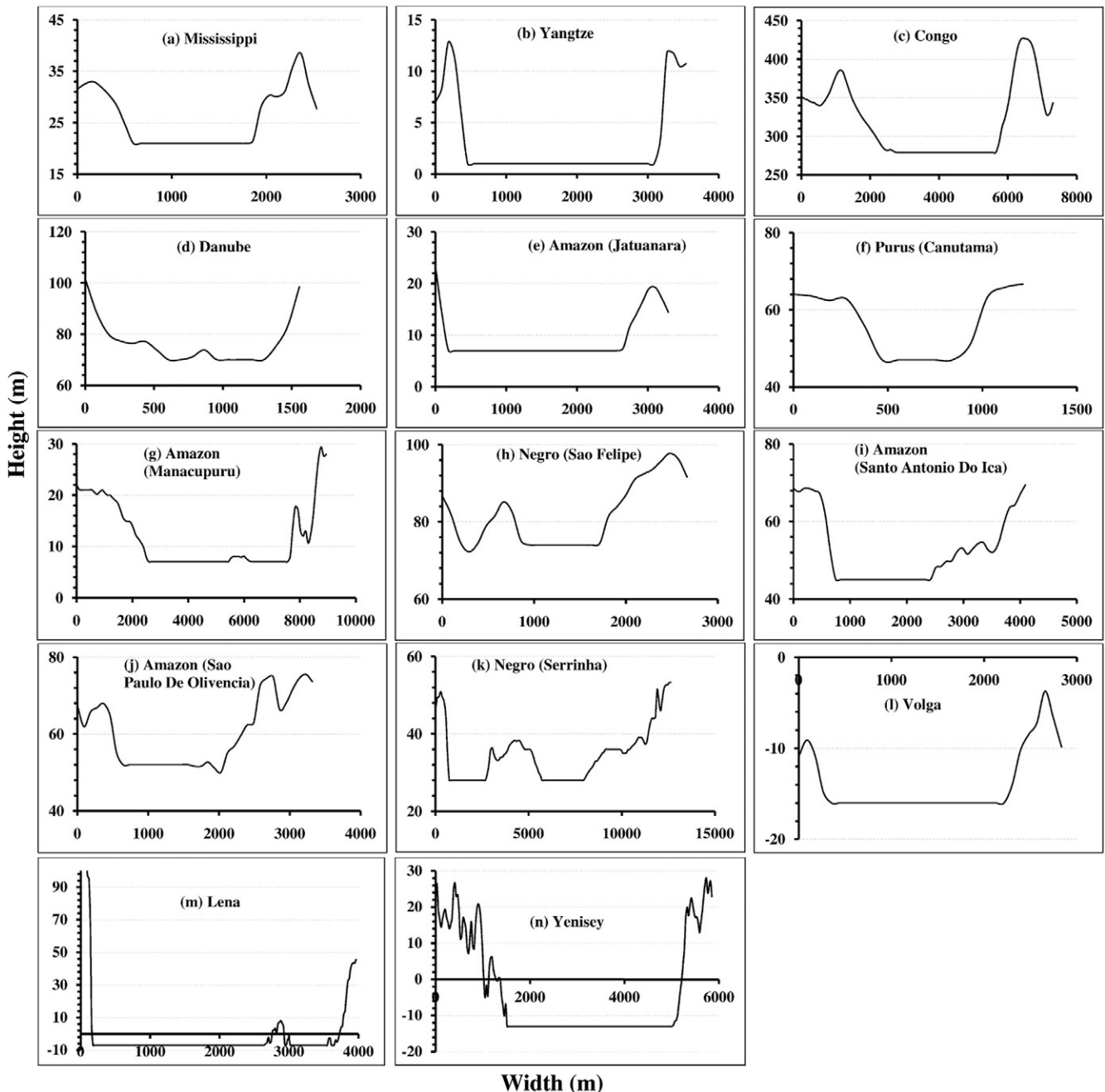
Fig. 4. River cross sections extracted from the ASTER Global Digital Elevation Model (ASTER GDEM) Version 2 data exhibiting the section type at the altimeter crossing site for the rivers (a) Mississippi, (b) Yangtze, (c) Congo, (d) Danube, (e) Amazon (Jatuanara), (f) Purus (Canutama), (g) Amazon (Manacupuru), (h) Negro (Sao Felipe), (i) Amazon (Santo Antonio Do Ica), (j) Amazon (Sao Paulo De Olivencia), (k) Negro (Serrinha), (l) Volga (m) Lena and (n) Yenisey.

Geophysiqueet Oceanographies Spatiales (LEGOS) in France (www.legos.obs-mip.fr/en/soa/hydrologie/hydroweb/) and the European Space Agency in collaboration with De Montfort University (tethys.eaprs.cse.dmu.ac.uk).

The Envisat and Jason-2 altimetry time series observations obtained from the databases represent heights with reference to the GRACE Gravity Model 02 (GGM02C). These values are obtained by defining virtual stations. Vegetation canopy and rough topography can cause errors in radar data. To address this challenge, Landsat data was used to define the water bodies accurately, thus minimizing the probability of non-water contamination in the altimetry measurement. The coordinates of the virtual station are then defined as the centroid of the selected altimeter observations within the defined water bodies. All the available

frequency data of a given cycle are then geographically averaged (Crétaux et al., 2011).

2.2.2. MODIS

The moderate-resolution imaging spectroradiometer (MODIS) is among the sensors on board the Earth Observing System (EOS) Terra (since 1999) and Aqua (since 2002) satellites. It is widely used for monitoring several terrestrial, atmospheric, and ocean phenomena due to its high spectral resolution of 36 bands ranging in wavelength from 0.4 μm to 14.4 μm, its moderate spatial resolution (2 channels at 250 m, 5 at 500 m, and 29 at 1 km), its high temporal resolution of 1–2 days with sometimes two passes during a day at mid-latitude (3 h apart from each other) (Friedl et al., 2010). Cloud free MODIS (MOD09GQ) surface

reflectance at full spatial resolution in Bands 1 and 2 were downloaded from https://lpdaac.usgs.gov at 35-day time steps; the days overlapping with the altimetry data. The high temporal resolution allows for extraction of daily effective river width measurements which ensures optimal utilization of the available altimetry data. The raw MODIS data in a sinusoidal projection was projected to Universal Transverse Mercator (UTM) at a spatial resolution of 250 m using the MODIS projection tool (MRT). The different behavior of water and land pixels in the Near Infrared (NIR) portion of the electromagnetic spectrum is exploited by considering Band 2 of the MOD09GQ data.

2.2.3. Digital Elevation Model (DEM)

In this study, the DEM was used to extract the river cross sections at the altimeter crossing point for all the rivers and to estimate river channel slope for the rivers within the Amazon Basin. In remote and data-scarce regions, high resolution DEMs are often not available or are costly to obtain. In these cases, it is necessary to evaluate lower resolution data for use (Jarihani, Callow, et al., 2015; Jarihani, Larsen, et al., 2015). We therefore adopted a 90 m DEM from CGIAR-CSI (http://srtm.csi.cgiar. org) whose accuracy over the Amazon basin has been previously evaluated as 5.51 m (LeFavour & Alsdorf, 2005). The 5-degree tile DEMs were mosaicked for each river basin over the altimetry crossing points for the defined river reaches.

In order to obtain reliable results, the slopes were defined over a long reach length as defined by (LeFavour & Alsdorf, 2005). Using a simple relationship developed by LeFavour and Alsdorf (2005), we determined the appropriate reach length (RL) as follows:

$$RL \approx \frac{2\sigma}{S_{min}} \qquad (6)$$

where S_{min} represents the minimum slope within the basin main stem (~1.5 cm/km), σ is the overall height error value (5.51 m). The DEMs were then projected to UTM. The slope was then computed by defining slope as the line of best fit for the elevations of the river centerline over the RL (Table 3). The elevation of the centerline for the defined river was derived in ArcGIS using the DEM (Fig. 2).

2.2.4. In situ discharge measurements

To establish the relations between the satellite and the in situ measurements, we used discharge measurements at the in situ ground observation sites to calibrate and validate our satellite derived measurements. The in situ observation data was obtained from the GRDC (GRDC, 2014).
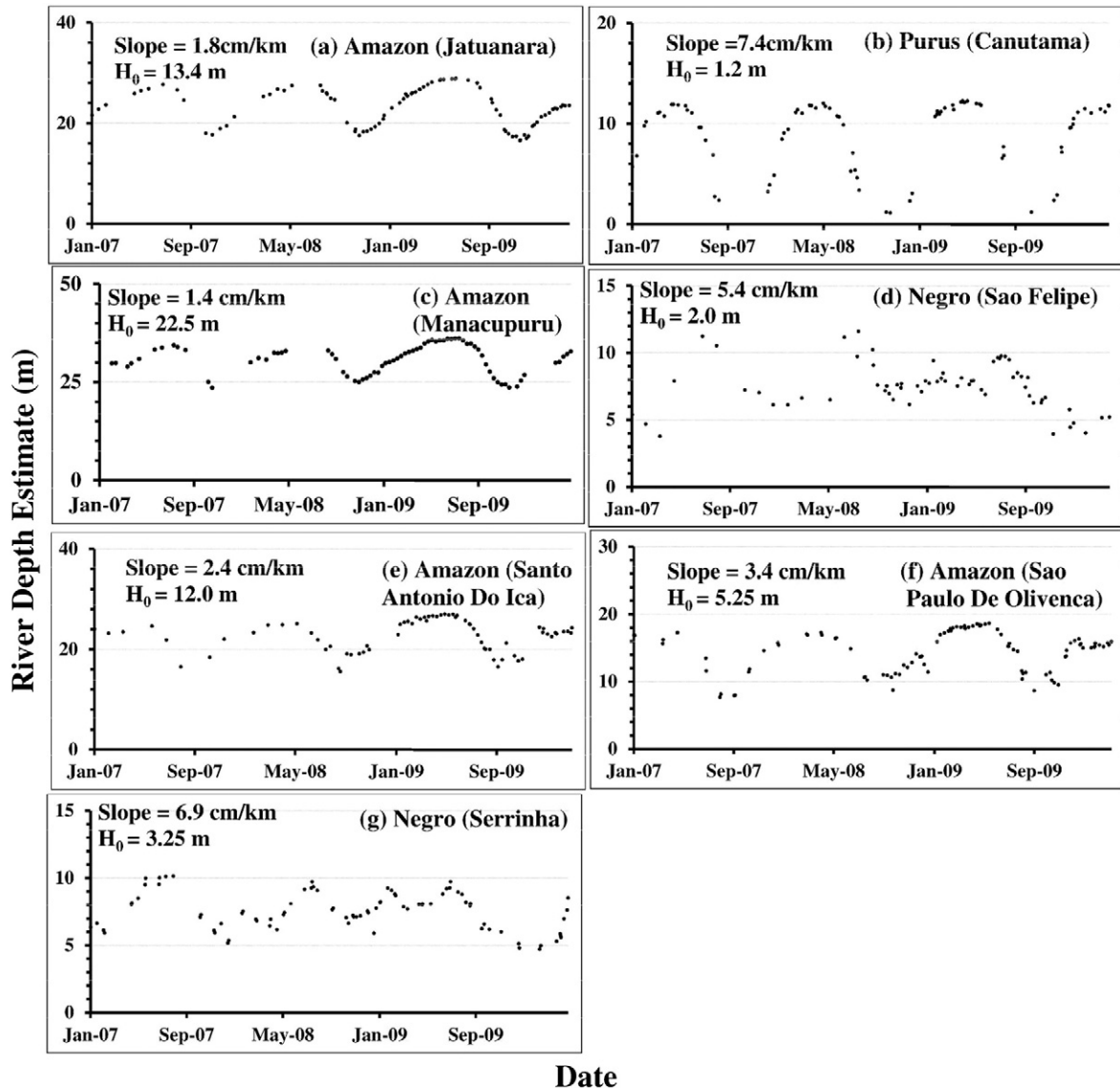

Fig. 5. Illustration of river depth estimates (Y) during 2007–2009. Slope is measured for the river segment at each station, and H_0 is used in estimating the river depth (Y).

2.3. Data overlay

Using the enhanced MODIS images (described in Section 2.2.2), we used ArcGIS to digitize the water surface areas at averaged river reach lengths that were approximately 10 times the river width (Bjerklie et al., 2005). Then the effective river width w_e measurements were computed using Eq. (7) (Sun, Ishidaira, & Bastola, 2010)

$$w_e = \frac{A_w}{l}. \qquad (7)$$

where A_w is the water surface area and l is the selected river reach length (Fig. 3).

3. Methods

3.1. Discharge estimation using stage versus using both stage and width

3.1.1. Development of the method

The satellite derived effective river width data (from MODIS) and its co-located stage measurements (from multiple missions in Table 2) are used. In this study, we examine two scenarios: discharge estimates
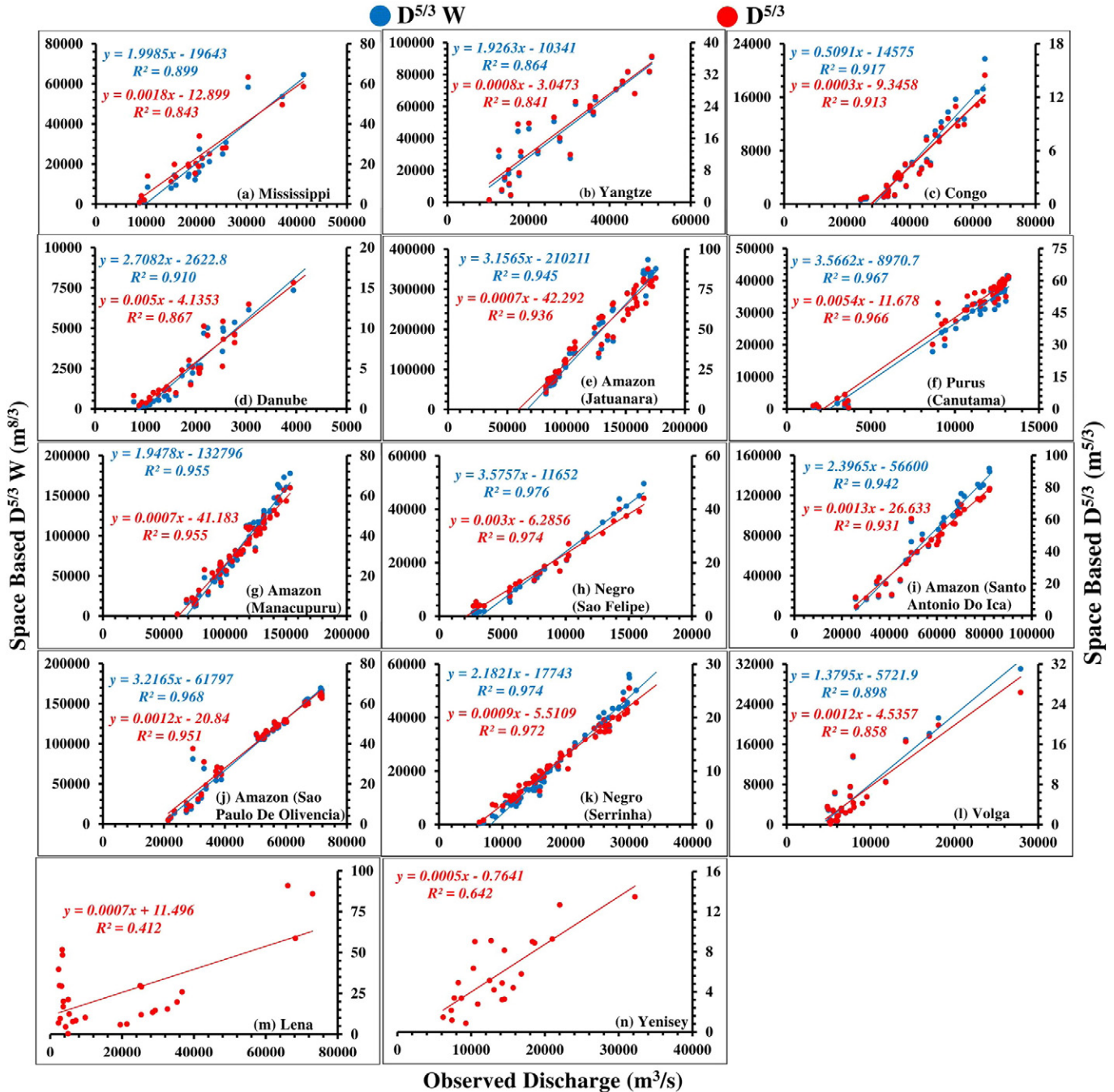

Fig. 6. Relationship between the satellite derived river stage and width ($D^{5/3}W$), left, river stage ($D^{5/3}$), right, and the in situ measured discharge, coinciding on the same day, during 2002–2006 (the calibration period), for the gauges at (a) Mississippi, (b)Yangtze, (c) Congo, (d) Danube, (e) Amazon (Jatuanara), (f) Purus, (g) Amazon (Manacupuru), (h) Negro (Sao Felipe), (i) Amazon (Santo Antonio Do Ica), (j) Amazon (Sao Paulo De Olivencia), (k) Negro (Serrinha), (l) Volga, (m) Lena, and (n) Yenisey. The stage and width ($D^{5/3}W$) observations for Lena River and the Yenisey River have not been included because the satellite images over the two rivers were affected, by ice, which prevented the river extends from being determined.

using only the river stage value and discharge estimates using both river stage and effective river width. In reality, a wide range of river channel cross-sections do exist (Fig. 4).

The discharge equation for a rectangular cross-section is as follows:

$$Q = \frac{S^{\frac{1}{2}}}{n} \frac{(W \cdot D)^{\frac{5}{3}}}{(W + 2D)^{\frac{2}{3}}}$$

(8)

where W is the river width, and D is the river stage.

The discharge equation for a trapezoid cross-section is as follows:

$$Q = = \frac{S^{\frac{1}{2}}}{n} \frac{\left(W \cdot D - D^2 \tan\theta^{-1}\right)^{\frac{5}{3}}}{\left(W + 2D \frac{1-\cos\theta}{\sin\theta}\right)^{\frac{2}{3}}}.$$

(9)

The discharge equation for an arc cross-section is as follows:

$$Q = \frac{S^{\frac{1}{2}}}{n} \frac{W \cdot D^{\frac{5}{3}} \left(\frac{1}{2} \cdot \left(\pi \cdot \frac{\alpha}{180} - \sin\alpha \cdot \cos\alpha\right)\right)^{\frac{5}{3}}}{\sin\alpha \cdot \left(\pi \cdot \frac{\alpha}{180}\right)^{\frac{2}{3}} (1-\cos\alpha)^{\frac{5}{3}}}.$$
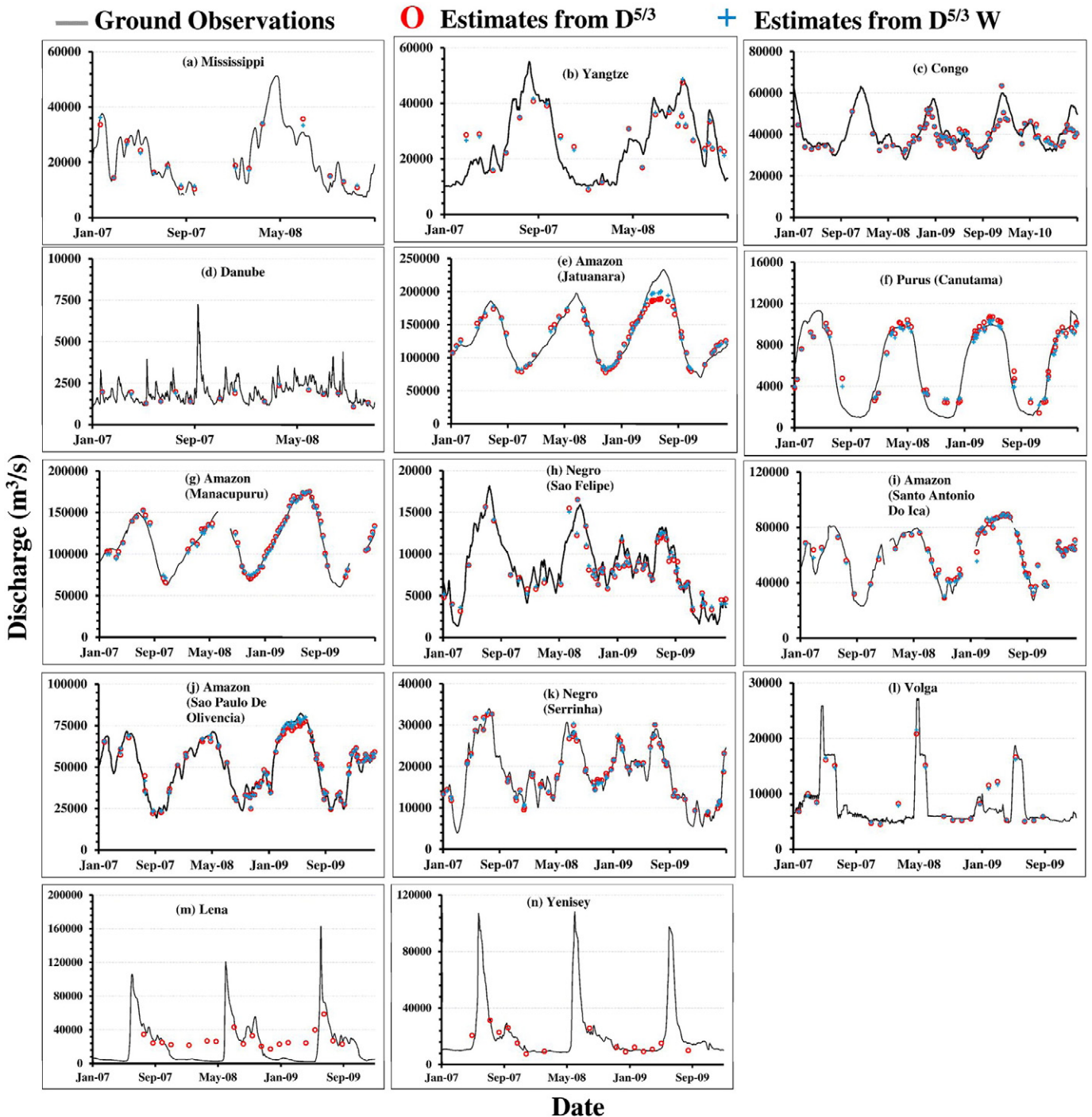
(10)

Fig. 7. Comparison of estimated stream flows from space-derived river stage alone and from space-derived river stage together with effective river width during 2007–2009, the validation period (see Table 4 for metrics).

Table 4
The performance evaluation results of the *NS*, *RMSE*, *RRMSE*, *RE* and R^2 when stage is used (columns 2–6) and when both stage and width are used (columns 8–12).

Site	Stage					Stage and width				
	NS	*RMSE* (m³/s)	*RRMSE* (%)	*RE* (%)	R^2	*NS*	*RMSE* (m³/s)	*RRMSE* (%)	*RE* (%)	R^2
Mississippi	0.94	2196.1	11.5	4.96	0.95	0.95	2140.4	11.2	4.47	0.96
Yangtze	0.52	8415.1	27.8	7.57	0.56	0.60	7733.0	25.5	7.07	0.64
Congo	0.58	5373.8	12.9	5.16	0.65	0.62	5113.2	12.2	4.98	0.70
Danube	0.55	316.11	17.3	7.10	0.63	0.69	261.15	14.3	6.65	0.77
Amazon (Jatuanara)	0.91	12,989	9.59	1.73	0.93	0.96	8915.7	6.58	0.72	0.97
Purus (Canutama)	0.86	1033.8	13.2	4.05	0.88	0.88	969.44	12.3	0.78	0.90
Amazon (Manacapuru)	0.96	5521.0	4.62	1.87	0.97	0.97	5070.3	4.24	0.97	0.97
Negro (Sao Felipe)	0.84	1334.2	15.0	6.71	0.87	0.88	1142.5	12.9	5.72	0.90
Amazon (Santo Antonio Do Ica)	0.95	4034.3	6.60	4.04	0.96	0.96	3473.7	5.68	1.28	0.97
Amazon (Sao Paulo De Olivencia)	0.96	3165.1	5.96	1.22	0.97	0.98	2461.0	4.63	0.64	0.98
Negro (Serrinha)	0.96	1293.3	6.68	0.96	0.96	0.97	1099.4	5.67	0.89	0.97
Volga	0.85	2668.1	24.2	2.62	0.85	0.89	1845.2	19.7	2.16	0.88
Lena	0.23	18,253	74.2	15.5		–	–	–	–	
Yenisey	0.71	3503.0	22.5	1.83		–	–	–	–	

For Eq. (10), if we consider both *W* and *D* as input parameters, *Q* is proportional to $W \cdot D^{\frac{5}{3}}$. For Eqs. (9) and (10), if the river is very wide, i.e., $W \gg D$, we can obtain the following equation (Eq. (11)) for both the rectangular and trapezoid cross-sections:

$$Q \approx \frac{S^{\frac{1}{2}}}{n} W \cdot D^{\frac{5}{3}}. \tag{11}$$

Therefore, in very wide river sections along large rivers, *Q* is approximately proportional to $D^{\frac{5}{3}}$ if we assume that *W* is a constant and only consider the single parameter *D* (Eq. (12)), and *Q* is proportional to $W \cdot D^{\frac{5}{3}}$ when we consider both *W* and *D* as variable parameters (Eq. (13)).

$$Q = k\left(D^{\frac{5}{3}}\right) + b, \tag{12}$$

$$\text{or } Q = k\left(W \cdot D^{\frac{5}{3}}\right) + b, \tag{13}$$

where, *k* (linear coefficient) and *b* (residual error) are parameters to be calibrated in the linear equation (rating curve for *Q*); and *b* accounts for all the approximations in the method.

3.1.2. Estimation of river stage

At a particular time, *t*, the river stage at a control section $D(t)$ can be estimated as follows:

$$D(t) = H(t) - H_m, \tag{14}$$

xwhere $H(t)$ is the water surface height calculated from multiple satellite altimetry data at the corresponding time, and H_m is the space-derived minimum water level according to the altimeter with reference to the GGM02C. Although the method developed by Rantz (1982) makes use of the discharge and the $H(t)$ values to estimate the height of zero flow (H_0), Leon et al. (2006) indicated that this methodology does not work for discharges in excess of 1000 m³/s as it fails to estimate values for H_0 that preserves the concept of a logarithmically linear stage discharge relationship. Leon et al. (2006) adopted a different approach that involves minimizing the root mean square error (RMSE) between the measured discharge and the rated discharge. To minimize the RMSE, the entire range of possible H_0 values must be defined. Our approach is more effective and does not require estimates of the H_0 value. From the altimetry dataset archive for 2002–2010, we considered the difference between H_m and $H(t)$ (as in Eq. (14)) as the river stage $D(t)$ (Fig. S1). The results from Fig. S1 are then used in Eqs. (12) and (13) on their own and in combination with the effective river width, respectively.

3.1.3. Discharge estimation using stage

First we establish the relationship between discharge and $D(t)$ for the entire study period. This allows us to identify the outliers and filter out erroneous data points. The data is then split into two time series for calibration and validation. In this case, a calibration against the ground observations is required to obtain a rating curve (optimizing *k* and *b*). The derived $D(t)$ is then substituted into the modified Manning's equation (Eq. (12)). The discharge data used in calibration is selected from the in situ stations that are closest to the virtual station (station under investigation; where the altimeter crosses). However, the closest virtual station from the in situ station ranged as far as 292 km in the case of Congo River (Table 2).

3.1.4. Discharge estimation using both stage and effective river width

In this case, the effective river width measurements (*W*) together with $D(t)$ are incorporated into Manning's equation (Eq. (13)). The parameters *k* and *b* are optimized using Eq. (13) for the calibration period of 2002–2006. A validation is then carried out using for the period of 2007–2010. The end period for the validation data varies depending on the available in situ observations.

The discharge estimates using stage (a methodology described in Section 3.1.3), and those using both stage and effective river width (a methodology described in Section 3.1.4) were then compared via plots.

3.1.5. Performance evaluation

To check the performance of the discharge estimates, we used the root mean square error (*RMSE*), Nash–Sutcliffe coefficient (*NS*) (Nash & Sutcliffe, 1970), relative root mean square error (*RRMSE*), and relative error (*RE*) as the evaluation criteria.

$$RMSE = \sqrt{\left(\frac{\sum(Q_m - Q_e)^2}{z}\right)}, \tag{15}$$

$$NS = 1 - \frac{(Q_m - Q_e)^2}{\left(Q_m - \overline{Q_m}\right)^2}, \tag{16}$$

$$RRMSE = \frac{RMSE}{\overline{Q_m}} \times 100\%, \tag{17}$$

$$RE = \frac{\sum_1^z Q_e - \sum_1^n Q_m}{\sum_1^n Q_m} \times 100\%, \tag{18}$$

where Q_m is the measured discharge, Q_e is the estimated discharge, $\overline{Q_m}$ is the mean measured discharge, and *z* is the number of observations. The values of *NS* range from $-\infty$ to 1. When *NS* is equal to one, it

represents a perfect match of the estimated discharge to the measured discharge.

We then evaluated the error contribution for each of the remote sensing derived parameters, i.e., Manning's roughness coefficient, the slope used in Eq. (11), and the stage and effective river width used in Eq. (13). The discharge error contribution from each parameter was obtained by varying the parameters by the measurement errors associated with each, i.e., Manning's roughness coefficient (± 0.003), slope (errors

in Table 3), effective river width is fixed to the remotely sensed pixel size (250 m), and the stage was varied by the standard deviation of the satellite altimetry observations from the given height.

3.2. Comparison of Model 1 and Model 2

We then carefully compared our methodology listed in Eq. (13) (hereinafter Model 1) with a previously developed statistically based
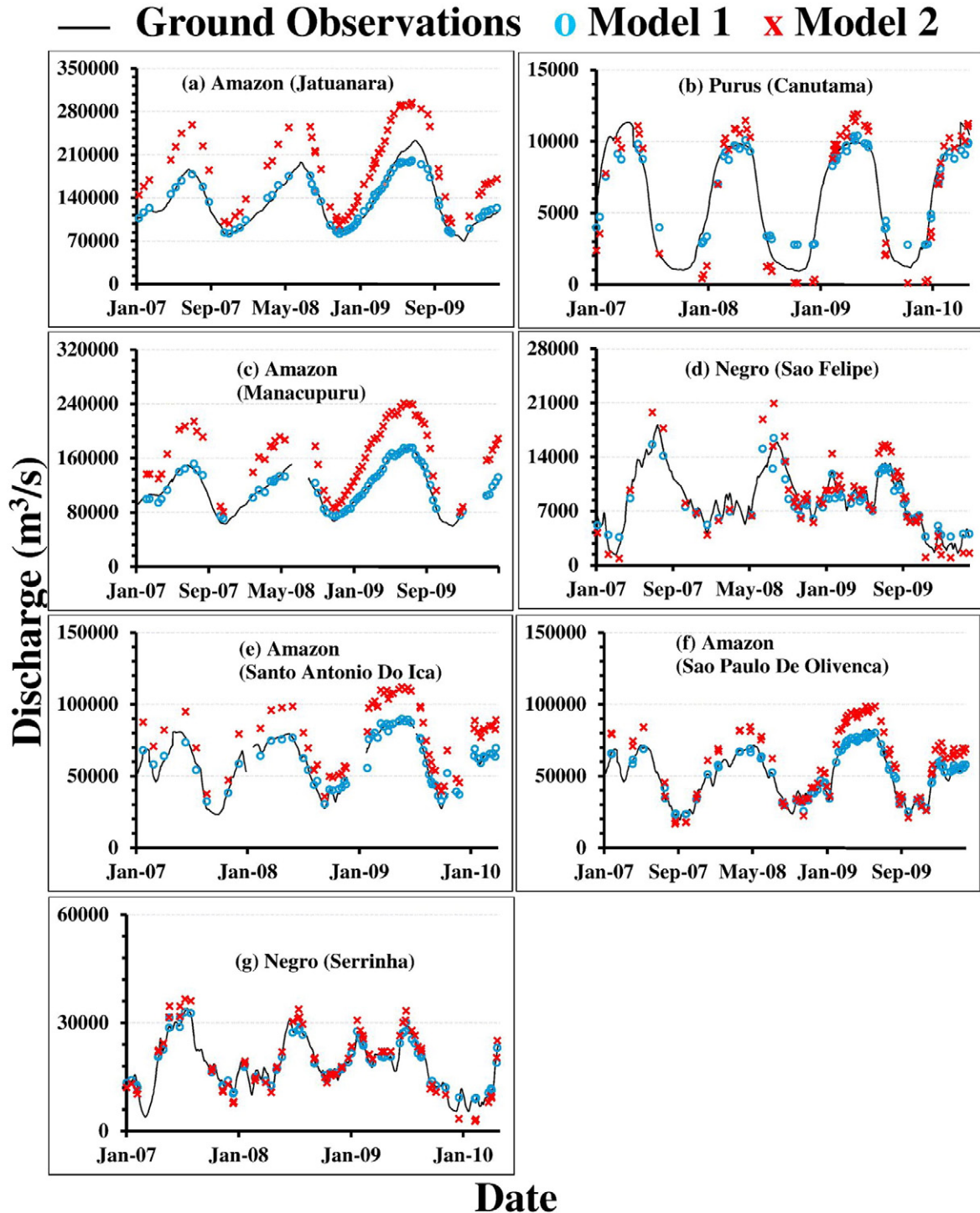

Fig. 8. Comparison of the discharge estimates using Model 1 (this study) and Model 2 (Bjerklie et al., 2003) for the discharge gauges in the Amazon River basin (see Table 5 for metrics). The comparison was carried out in the amazon because a tested roughness coefficient value by LeFavour and Alsdorf (2005) is available.

Table 5
The performance evaluation results of the *NS*, *RMSE*, *RRMSE*, *RE* and R^2 in Model 1 (columns 2–6) and Model 2 (columns 8–12).

Site	Model 1						Model 2				
	NS	*RMSE* (m³/s)	*RRMSE* (%)	*RE* (%)	R^2		*NS*	*RMSE* (m³/s)	*RRMSE* (%)	*RE* (%)	R^2
Amazon (Jatuanara)	0.96	8915.7	6.58	0.72	0.97		−0.64	55,341	40.9	27.5	0.96
Purus (Canutama)	0.88	969.44	12.3	0.78	0.90		0.72	1625.4	21.2	5.43	0.90
Amazon (Manacupuru)	0.97	5070.3	4.24	0.97	0.97		−0.45	56,707	47.4	31.6	0.96
Negro (Sao Felipe)	0.88	1142.5	12.9	5.72	0.90		0.69	1849.0	20.8	2.03	0.93
Amazon (Santo Antonio Do Ica)	0.96	3473.7	5.68	1.28	0.97		−0.20	21,457	35.1	23.6	0.96
Amazon (Sao Paulo De Olivencia)	0.98	2461.0	4.63	0.64	0.98		0.56	11,280	21.2	13.8	0.98
Negro (Serrinha)	0.97	1099.4	5.67	0.89	0.97		0.86	2448.8	12.6	1.99	0.97

multivariate discharge estimation equation (Eq. (19), hereinafter Model 2) (Bjerklie et al., 2003) that has been tested for the Mekong and Ob Rivers (Birkinshaw et al., 2014).

$$Q = 7.22W^{1.02}Y^{1.74}S^{0.35}, \qquad (19)$$

where *W* is effective river width obtained from MODIS images. Different from *D* used in Model 1 (see Eqs. (12) and (13)), *Y* is the river depth estimate and is calculated as follows.

$$Y(t) = H(t) - H_0, \qquad (20)$$

where H_0 is the height of zero flow (Leon et al., 2006). *S* is the river slope (from Section 2.2.3), which changes with distance downstream, i.e., the gradient is steep in the head waters and gentler downstream. To account for variations in slope steepness, we compute *S* over a long river section (over which discharge gauges are located) to reduce the error (LeFavour & Alsdorf, 2005).

The steps involved in comparing Model 1 with Model 2 are detailed as follows:

(1) Model 1 adopts Eq. (13), in which the slope and roughness coefficient are assumed constant and only the satellite derived parameters (i.e., river width and river stage) are used for discharge estimation.

(2) We use Eq. (11) to estimate river depth (*Y*) for Model 2 (Eq. (19)). Herein, all the parameters of Eq. (11) are determined/obtained from a 90 m digital elevation model (slope), satellite images (river width, river stage), and the literature (roughness coefficient) (Albertson & Simons, 1964). We use a value of 0.025 as the typical roughness coefficient subject to an error of ±0.003 according to LeFavour and Alsdorf (2005). Using Eq. (11), the river depth (*Y*) (Fig. 5) is estimated by minimization of the *RRMSE* between the observed (in situ station) and estimated discharges (Leon et al., 2006).

The minimization of the error is performed by adding successive values of river depth at an interval of 0.1 m towards an estimated height of effective zero flow (H_0; see Fig. S2).

(3) Using the estimated *Y* (Fig. 5), the effective river width, and the slope, discharge estimates using Model 2 were then computed.

4. Results

4.1. Discharge estimation using stage versus using both stage and width (Model 1)

Figure S1 shows the time series for river stage (*D*) for the entire study period from 2002 to 2009. In the Fig. 6, the estimates from stage (right) and estimates from the stage + the effective river width (left) are calibrated against the ground-observed discharges to provide the discharge estimation equations for each gauge.

The determination coefficients were found to be lower in the Arctic rivers compared to the other studied rivers, with 0.41 for the Lena and 0.64 for the Yenisey (Fig. 6m and n).

The two empirical values (*k* and *b*) for each of the tested rivers are shown in Fig. 6. The two constants are site specific and may vary if different calibration data is used.

The coefficient of determination (R^2) values are high, and most values are >0.90. Fig. 7 shows the validations for the remotely-sensed discharge estimation equations with *D* and with both *D* and *W*. Despite the high R^2 values obtained from one-parameter (*D*) discharge estimation equations, inclusion of both the river stage and width (*D* and *W*) values leads to increases in the coefficient values and improvements in the resultant *NS* values.

The *NS* values for rivers with lower accuracies are observed to increase when the width values are incorporated; for example, the *NS* value changes from 0.55 to 0.69 for the Danube and 0.52 to 0.60 for the Yangtze (Table 4). The resultant time series estimates generate *NS* values

Table 6
Estimated resultant errors associated with the parameters stage and width using Model 1.

River	Stage				Width			
	RE (±%)	*NS* (±)	*RMSE* (± m³/s)	*RRMSE* (±%)	*RE* (±%)	*NS* (±)	*RMSE* (± m³/s)	*RRMSE* (±%)
Mississippi	0.38	0.01	18.60	0.10	13.4	0.14	1920.7	10.0
Yangtze	13.1	0.11	1824	4.50	6.84	0.04	760.60	3.70
Congo	0.18	0.00	13.00	0.03	5.18	0.12	1253.6	3.10
Danube	0.30	0.02	7.810	0.50	19.0	1.07	293.30	16.1
Amazon (Jatuanara)	0.06	0.01	18.00	0.02	3.05	0.02	1032.0	0.73
Purus (Canutama)	0.20	0.03	103.8	1.40	18.7	0.50	1333.9	18.8
Amazon (Manacupuru)	0.09	0.00	24.60	0.02	4.13	0.05	3321.6	2.78
Negro (Sao Felipe)	5.38	0.07	267.2	3.30	13.8	0.28	881.18	10.9
Amazon (Santo Antonio Do Ica)	2.14	0.02	757.7	1.28	7.73	0.12	3682.0	6.28
Amazon (Sao Paulo De Olivencia)	0.53	0.00	56.90	0.13	4.19	0.04	850.20	1.73
Negro (Serrinha)	0.35	0.01	21.30	0.20	5.91	0.05	505.90	2.80
Volga	1.05	0.01	61.00	0.70	11.8	0.11	809.40	8.70

Table 7
Estimated resultant errors associated with the parameters roughness coefficient and slope using Eq. (11).

River	Roughness coefficient				Slope			
	RE ($\pm$%)	NS ($\pm$)	RMSE ($\pm$m^3/s)	RRMSE ($\pm$%)	RE ($\pm$%)	NS ($\pm$)	RMSE ($\pm$m^3/s)	RRMSE ($\pm$%)
Amazon (Jatuanara)	9.90	0.15	7528.0	5.32	4.30	0.04	9680.9	1.56
Purus (Canutama)	20.5	0.41	1122.7	15.8	14.7	0.15	589.40	8.40
Amazon (Manacupuru)	11.8	0.24	23,019	16.2	3.67	0.16	15,392	12.9
Negro (Sao Felipe)	9.60	0.30	1353.2	16.7	4.39	0.12	709.78	8.80
Amazon (Santo Antonio Do Ica)	11.7	0.22	7965.0	13.5	5.69	0.06	3586.8	6.08
Amazon (Sao Paulo De Olivencia)	5.70	0.24	3961.1	8.23	9.46	0.09	1639.9	3.43
Negro (Serrinha)	17.0	0.31	2688.2	14.4	2.15	0.06	822.10	4.40

of 0.23 and 0.71 for the Lena and Yenisey Rivers, respectively, with the majority of the inaccurate estimates occurring in the colder seasons.

4.2. Comparison between Model 1 and Model 2

Model 1 produces Nash–Sutcliffe efficiency values that range between 0.60 and 0.97, indicating that it is a quality discharge estimation equation. From the results in Fig. 8, estimates from Model 2 correlate well for the stations that have average discharges <20.000 m^3/s.

Significant errors were found for stations on the Amazon where the discharges are >50.000 m^3/s (see Fig. 8; Table 5).

Furthermore, there is a tendency for overestimation by Model 2, and the accuracy decreases as the river discharge increases. For example, Model 2 has the largest errors at the Jatuanara (128,286 m^3/s), Manacupuru (110,234 m^3/s), and Santo Antonio Do Ica stations (57,984 m^3/s) of the Amazon River (Fig. 8).

4.3. Sensitivity analysis

The analysis of the error in the stage and width parameters used in Model 1 indicates that their performances varied between different one river sections. Generally, errors in river width measurements are larger than errors in satellite derived river stage (Table 6). Rivers with the least discharge are observed to have higher width measurement errors, i.e., Danube, Purus, and Negro. Errors in stage depend on the standard deviation of each satellite altimetry measurement from the given height. The Yangtze River had the highest stage error (Table 6).

An evaluation of the errors associated with the roughness coefficient and slope for Eq. (11) are presented in Table 7. Varying the roughness coefficient by the given error margin ($\pm$0.003) results in large errors compared to the variation of slope errors (Table 7).

5. Discussion

5.1. Discharge estimation using stage versus using both stage and width

Model 1 is shown to be an accurate discharge estimation equation that uses river stage and width (D and W) to optimize the unknown parameters k and b. It provides an ideal method for estimating river discharge for a wide range of river channels, including the flat terrains/river sections in the study region (Jarihani, Callow, et al., 2015; Jarihani, Larsen, et al., 2015). The results of our study correspond with previous works that report higher accuracy in discharge estimation models that include more than one discharge estimation parameters (width, stage, and slope) compared to models that use width or stage only (Bjerklie et al., 2003, 2005). However, this paper is the first to show that river discharge estimates using stage and effective river width (D and W) derived using remote sensing outperform studies with single discharge estimate parameters (Birkinshaw et al., 2010; Leon et al., 2006; Smith & Pavelsky, 2008; Tarpanelli et al., 2013). The Nash–Sutcliffe efficiency values range between 0.60 and 0.97, and the majority of the rating curves had R^2 values >0.90. In Model 1, the temporal change in discharge is shared between the temporal adjustment in width and stage. This possibility assumes a constant roughness coefficient and river slope represented by k. Therefore, by calibrating the data using the 2002–2006 time series observations, the unknown k and b factors are optimized. Some of the parameters accounted for by the factors k and b can be approximated in some instances. However, numerous errors would be inevitable. For instance, slope could be estimated using satellite altimetry but major assumptions have to be made. Birkinshaw et al. (2014) estimated slope using the satellite altimetry crossing (at the location where the discharge is to be estimated) and the next downstream altimetry crossing site. The crossing days at the upstream and downstream sites differ and this may result to inconsistencies in height determination. The river slopes derived from DEMs have associated errors as well (LeFavour & Alsdorf, 2005). In this study, Model 2 uses slope estimates from a DEM, which results which results in error values presented in Table 7 whose averaged values give a RE of 6.43%, NS of 0.10, RMSE of 4631 m^3/s and RRMSE of 6.51%. Mean velocity derived from river surface velocity using SAR has also been previously investigated (Bjerklie et al., 2005). However, estimating surface velocity is limited to channels where the effects of wind speed and direction can be adequately corrected (Bjerklie et al., 2005; Grünler, Romeiser, & Stammer, 2013; Plant, Keller, & Hayes, 2005). An additional limitation is that surface velocity data may only be available on an occasional basis depending on the orbits of satellites and sensor availability which can result in a temporal mismatch with the altimetry

Table 8
A table summarising the error sources/uncertainties in the present study and their general classification.

Error/uncertainty source	Magnitude	Reason
Stage	Low to medium	Temporal resolution
Width	Low to medium	Spatial resolution
Slope	Low to medium	Spatial resolution
Velocity	High	Significant limitations are inherent in velocity estimate using SAR (LeFavour & Alsdorf, 2005; Plant et al., 2005).
Discharge measurements and curve rating	Low	Studies indicate a limited contribution of between 6% and 20% (Herschy, 2002; Leonard et al., 2000; Pelletier, 1988)
Lateral flow	Low–medium	In the present study the comparison is carried out up to 292 km without loss of generality. However, the presence of tributaries and outflow would increase the error.
Roughness coefficient	Medium	A general classification is used based on the river conditions

data. In contrast, our methodology uses MODIS which has a wider coverage and a higher temporal resolution. This ensures spatial and temporal consistency between the Envisat and MODIS datasets. With the forthcoming Surface Water Ocean Topography (SWOT) mission, the concurrent collection of stage and river width will become possible (Pavelsky & Durand, 2012).

On Fig. 6, the temporal change in discharge that depends on the variations in stage alone i.e. $D^{5/3}$, is a concept previously investigated (Birkinshaw et al., 2010; Tarpanelli et al., 2013). This possibility assumes, in addition to the roughness coefficient and river slope, that the river width is constant. This assumption is another potential source of error owing to the fact that in arc and trapezoidal cross-sections temporal changes in river discharge reflects changes in width. The changes in river width explain why the results presented in Fig. 7 gives better estimates using $D^{5/3}W$ than $D^{5/3}$ in Fig. 6. The averaged values of the RE reduce from 4% using stage to 3.02% using both stage and width (Table 4).

We have applied our method to fourteen virtual stations in eight river basins with different channel widths and different climates. Results from the rivers in the higher latitudes show that most of the outliers are measurements taken during winter. The radar echoes are often affected by snow and ice cover during winter (Kouraev, Zakharova, Samain, Mognard, & Cazenave, 2004). As a consequence, the resultant radar waveform may not exhibit the simple broad-peaked shape typical of water surfaces. The waveforms in these situations can instead be complex and multi-peaked. As we move into the Arctic, the R^2 values are lower for the Lena and Yenisey Rivers; these rivers are mostly covered with ice for half of the year. A plot of the validation demonstrates agreement between the ground observations and the satellite-derived estimates. However, from November to April, the ground recorded discharge values are lower than the satellite-derived values. This coincides with the regional cold season when the river is frozen. The characteristics of the altimetry echoes depend on the volume scattering effect of the media and the two-way attenuation of the return signal. According to Papa, Legresy, Mognard, Josberger, and Remy (2002), the presence of ice and snow attenuates the altimeter measurements, thereby influencing the radar waveform and backscatter values. This may account for the lower accuracies of the estimates in the Lena and Yenisey Rivers.

5.2. Comparison between Model 1 and Model 2

Models 2 is a statistically based estimation method that depends on the ability to translate stage, coupled with other observable characteristics, into the average water depth of a river channel. This study and previous research suggest that the performance of Model 2 varies for different rivers (Bjerklie et al., 2003; Negrel et al., 2011). According to Bjerklie et al. (2003), the accuracies in Model 2 range within approximately ±50% for 2/3 of the study period. In the current study, Model 2 reduces the error observed in the channels with discharges >50.000 within the Amazon basin. For basins with discharge less than ~20,000 m³/s, Models 1 and 2 are observed to correlate favorably and exhibit high NS values. These results are in agreement with the results of a previous study where the performance of Model 2 was tested in the Mekong and Ob rivers with discharges of 16,000 m³/s and 12,800 m³/s, respectively (Birkinshaw et al., 2014). With the current limitation in remote sensing capabilities, some parameters, such as the roughness coefficient, cannot be accurately estimated for each channel section. A sensitivity analysis carried out using the stated roughness coefficient error of ±0.003 contributes to errors presented in Table 7 whose averaged values give a RE of 12.3%, NS of 0.27, RMSE of 6805 m³/s and RRMSE of 12.9%. Therefore, errors in estimating the roughness coefficients for each channel would lead to even higher error contributions. In contrast, Model 1 optimizes unknown k and b factors for each river channel depending on the characteristics of the channels' width and stage. This results in Model 1 exhibiting reduced errors for large rivers. Additionally, a constant value for the river slope is used in Model 2 implying that it is a geomorphic characteristic of the river. A sensitivity analysis carried out by varying the slope values by the respective errors presented in Table 3 shows that the error changes could translate to a mean average RE of 6.43% (Table 7). Therefore, temporal variations in river slope could potentially introduce substantial errors in the estimation of slopes which translate to errors in discharge estimates. At present, extracting the temporal variations in water surface slope is still a challenge. Similarly, related studies adopt a constant slope either from an SRTM DEM averaged over a long river length or by taking measurements at the satellite altimetry crossing points (at the location where the discharge is to be estimated) and the next downstream altimetry crossing site (Birkinshaw et al., 2014).

5.3. Error evaluation

Alsdorf et al. (2007), Bjerklie et al. (2003), and Tang et al. (2009) have investigated remote sensing data sources and their potential use for measuring river stage, effective river width, velocity, and slope. A number of different techniques have made use of these remote sensing data sources to estimate river discharge (as outlined in Table 1). To our knowledge, this is the first study to highlight the possibility of improving discharge estimations via satellite derived river stage and effective river width information. That being said, there are uncertainties associated with Model 1. The variability in accuracy values may reflect the spacing between the in situ measurement stations and the virtual stations. This can result from lateral river flow from sub-catchments between stations (Table 2). In general, the estimated discharge values correspond well with the in situ measurements. Therefore, by using remote sensing data, we can reduce the distance between virtual and real gauge stations, which ranges up to 292 km in the current study. Additional errors emanate from the uncertainty in discharge measurement and the curve fitting procedures, which have been reported in some studies (Peña-Arancibia et al., 2015; Tomkins, 2014). According to Herschy (2002) and Leonard, Mietton, Najib, and Gourbesville (2000), the errors in discharge measurements are approximately 6% of the flow value provided by the current meter. Pelletier (1988) reviewed >140 publications and reported that the uncertainty of discharge measurements might be as high as 20% of the observed value and is dependent on many operational factors, e.g., number of verticals and sampling points, current velocity, exposure time of instruments, and location of gauged section. The size of the aforementioned satellite footprint limits the retrieval of stage data using this method to rivers with widths greater than ~800 m (Birkett & Beckley, 2010; Sulistioadi et al., 2015). Radar signals returned by water bodies smaller than 800 m are more likely to be contaminated by non-water surfaces, which may degrade the measurement quality. An assessment of the discharge errors associated with the quality of the altimetry derived stage measurements in Table 6 indicate that these errors are minimal. This is possibly because the study rivers meet the minimum river width requirement.

The MODIS data used in measuring the effective river width is limited by its spatial resolution, i.e., 250 m. Because the width error is fixed to the remotely sensed pixel size, width accuracies improve with increasing channel width. This explains why in Table 6 rivers with less discharge have relatively larger discharge uncertainties associated with river width. This contributes to an averaged RE of 9.48% in river width measurement (Table 6). This averaged value of uncertainty is higher than the averaged ~1% recorded improvement using both stage and width. From Tables 2 and 6, its observed that rivers with <21.415 m³/s discharge have relatively high uncertainty in river width measurements therefore contributing to the high uncertainty in river width measurements. On the other hand, rivers with >21.415 m³/s discharge have lower uncertainty in river width measurements in the present study. This is logical, as large width errors can cause some cross sections to show an increase in width while others; resulting in larger uncertainties over narrower rivers. The uncertainty in river width measurements could be improved by considering high spatial resolution satellite images; especially for the narrower rivers. Additional effective river

width error includes human induced method error associated with effective river width measurement. A previous study reported that this source of error ranged within 0.1–13%, with an average error of 3% (Smith, Isacks, Bloom, & Murray, 1996). Finally, Model 1 assumes that the temporal difference between the datasets, i.e., the instantaneous observations made from MODIS, Envisat, and Jason-2 in relation to the in situ measurements from relatively continuous values, leads to negligible changes in the observations. Even though all the observations are made within the same day, this difference in the dataset may contribute to errors.

From the error analysis in the present study (Tables 7 and 8) and other studies carried out within this area of study, we broadly classify the errors and uncertainties within discharge estimation (Table 8). The classification gives a level of uncertainty, i.e., low, medium, and high uncertainty (related to the error budget), and an underlying reason.

6. Conclusion and recommendation

In this paper, we demonstrated a methodology for using remotely-sensed parameters to estimate discharge. Specifically, the satellite altimetry height, either in isolation or in combination with the remotely-sensed river width measurements, are the key parameters used. Our methodology can be used to fill gaps in the existing discharge databases and provide an alternative for ground observation sites which are no longer operational. Results from this study also indicate that discharge estimates incorporating effective river width from MODIS outperform the estimates that only utilize satellite altimetry data. Additionally, for the rivers in higher latitudes, the altimeter observations made during winter lie far from the trend lines. This agrees with Kouraev et al. (2004) which reported that snow and ice can influence the measurements of water surface heights.

We have proved that Model 1 which utilizes width and stage to optimize the unknown k and b factors is applicable. However, Model 1 would have broader and more practical application if all the parameters could be estimated without calibration of the in situ measurements. Additionally, the temporal resolution remains the major challenge in using satellite altimetry for monitoring water stage. Clearly, the 35-day period for Envisat and the 10-day period for Jason 2, cannot completely replace daily observations taken at ground observation gauges around the world. However, the upcoming missions (Jason-3, Jason CS, Sentinel-3a and b, and SWOT) will likely mitigate this issue.

Model 2, a previously tested approach, gives reasonable estimates for the Amazon tributaries. However, it largely overestimates discharges for the main stream of the Amazon River. Model 1 developed in this study shows a consistently higher accuracy in estimating the river discharges in both the tributaries and the main stream of the Amazon River. It could be applied to large rivers, such as the Amazon and the Congo, to avoid overestimates that result in Model 2.

Appendix A. Derivation of general equations for discharge estimation from space derived parameters

We begin with Manning's equation:

$$v = \frac{k_n}{n} R^{\frac{2}{3}} S^{\frac{1}{2}} \tag{A1}$$

where, V is the cross-sectional average velocity, $k_n = 1$ for the international system of units, R is the hydraulic radius ($= A / P_{\text{wet}}$), and S is the slope of river bed.

We then derive the space derived discharge estimation equations as below; first Eq. (A1) is expressed in terms of $\frac{q}{A}$ is in Eq. (A2):

$$\frac{q}{A} = \frac{1}{n} R^{\frac{2}{3}} S^{\frac{1}{2}} \tag{A2}$$

where, n is the roughness coefficient; A is the cross sectional area of the river; P_{wet} is the wetted perimeter (total length of stream bed from one bank to the opposite bank); R is the hydraulic radius ($= A / P_{\text{wet}}$); and S is the slope of river bed. Substituting for the hydraulic radius in Eq. (A2), we can obtain Eq. (A3) as follows:

$$q = \frac{1}{n} A \left(\frac{A}{P_{\text{wet}}} \right)^{\frac{2}{3}} S^{\frac{1}{2}}. \tag{A3}$$

We consider three ideal river cross-sections when deriving the equations: rectangular, trapezoidal, and arc (Fig. A1).

A.1. Rectangular cross-section (Fig. A1a)

By substituting Eqs. (A4) and (A5) in (A3) we obtain Eq. (A6):

$$P_{\text{wet}} = W + 2D \tag{A4}$$

$$A = W \cdot D \tag{A5}$$

$$q = \frac{S^{\frac{1}{2}}}{n} \frac{(W \cdot D)^{\frac{5}{3}}}{(W + 2D)^{\frac{2}{3}}} \tag{A6}$$
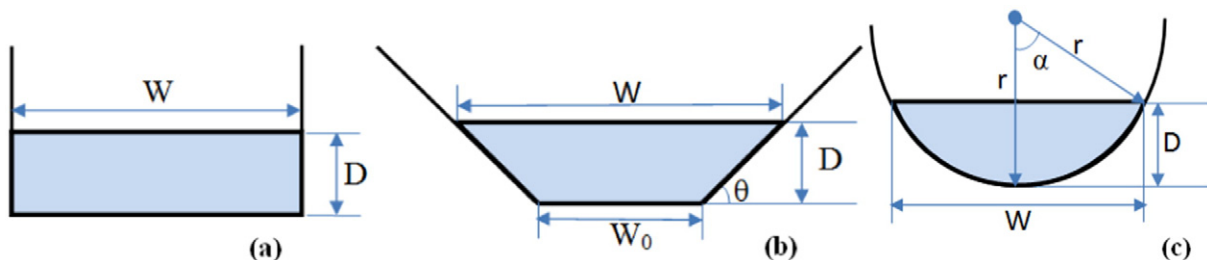

Fig. A1. Three ideal river cross-sections.

where, W is space derived river width and D is the river water depth that can be obtained from river stage data.

A.2. Trapezoid cross-section (Fig. A1b)

For trapezoidal sections, substituting Eqs. (A7) and (A8) in (A3) we obtain Eq. (A9):

$$P_{\text{wet}} = W + 2D\frac{1 - \cos\theta}{\sin\theta} \tag{A7}$$

$$A = \left(W - D\tan\theta^{-1}\right) \cdot D \tag{A8}$$

$$q = \frac{S^{\frac{1}{2}}}{n} \frac{\left(W \cdot D - D^2 \tan\theta^{-1}\right)^{\frac{5}{3}}}{\left(W + 2D\frac{1-\cos\theta}{\sin\theta}\right)^{\frac{2}{3}}}. \tag{A9}$$

A.3. Cross-section (Fig. A1c).

Finally in arc sections, substituting Eqs. (A10) and (A11) in (Eq. (A3)) we obtain Eq. (A12):

$$P_{wet} = \pi r \cdot \frac{\alpha}{90} \tag{A10}$$

$$A = r^2\left(\pi \cdot \frac{\alpha}{180} - \sin\alpha \cdot \cos\alpha\right) \tag{A11}$$

$$q = \frac{S^{\frac{1}{2}}}{n} \frac{W \cdot D^{\frac{5}{3}}\left(\frac{1}{2} \cdot \left(\pi \cdot \frac{\alpha}{180} - \sin\alpha \cdot \cos\alpha\right)\right)^{\frac{5}{3}}}{\sin\alpha \cdot \left(\pi \cdot \frac{\alpha}{180}\right)^{\frac{2}{3}}(1 - \cos\alpha)^{\frac{5}{3}}}. \tag{A12}$$

For Eq. (A12), q is proportional to $W \cdot D^{\frac{5}{3}}$ if we consider two parameters.

If we consider only one parameter D, then Eq. (A12) can be converted to Eq. (A13):

$$q = 2\frac{S^{\frac{1}{2}}}{n} \frac{D^{\frac{8}{3}}\left(\frac{1}{2} \cdot \left(\pi \cdot \frac{\alpha}{180} - \sin\alpha \cdot \cos\alpha\right)\right)^{\frac{5}{3}}}{\left(\pi \cdot \frac{\alpha}{180}\right)^{\frac{2}{3}}(1 - \cos\alpha)^{\frac{8}{3}}}. \tag{A13}$$

For large rivers $W \gg D$, in our case $W > 800$ m, we could get the equation below (Eq. A14) from all the cases (Eqs. (A6), (A9), and (A12)).

$$q \approx \frac{S^{\frac{1}{2}}}{n} W \cdot D^{\frac{5}{3}} \tag{A14}$$

Therefore, in very wide river sections along large rivers, q is approximately proportional to $W \cdot D^{\frac{5}{3}}$ if we consider two parameters, and q is approximately proportional to $D^{\frac{5}{3}}$ if we assume W as a constant and only consider the parameter D (K is considered as a constant, $K = \frac{S^{1/2}}{n}$).

$$q \approx KW \cdot D^{\frac{5}{3}} \tag{A15}$$

Appendix B. Supplementary data

Supplementary data to this article can be found online at http://dx.doi.org/10.1016/j.rse.2016.03.019.

References

Albertson, M. L., & Simons, D. B. (1964). Fluid mechanics. *Handbook of applied hydrology: A compendium of water-resources technology.* New York: McGraw-Hill.

Alsdorf, D. E., Rodríguez, E., & Lettenmaier, D. P. (2007). Measuring surface water from space. *Reviews of Geophysics, 45*(2) (n/a-n/a).

Birkett, C. M., & Beckley, B. (2010). Investigating the performance of the Jason-2/OSTM radar altimeter over lakes and reservoirs. *Marine Geodesy, 33*(Suppl. 1), 204–238.

Birkinshaw, S. J., Moore, P., Kilsby, C. G., O'Donnell, G. M., Hardy, A. J., & Berry, P. A. M. (2014). Daily discharge estimation at ungauged river sites using remote sensing. *Hydrological Processes, 28*(3), 1043–1054.

Birkinshaw, S. J., O'Donnell, G. M., Moore, P., Kilsby, C. G., Fowler, H. J., & Berry, P. A. M. (2010). Using satellite altimetry data to augment flow estimation techniques on the Mekong River. *Hydrological Processes, 24*(26), 3811–3825.

Bjerklie, D. M., Lawrence Dingman, S., Vorosmarty, C. J., Bolster, C. H., & Congalton, R. G. (2003). Evaluating the potential for measuring river discharge from space. *Journal of Hydrology, 278*(1–4), 17–38.

Bjerklie, D. M., Moller, D., Smith, L. C., & Dingman, S. L. (2005). Estimating discharge in rivers using remotely sensed hydraulic information. *Journal of Hydrology, 309*(1–4), 191–209.

Brakenridge, G. R., Nghiem, S. V., Anderson, E., & Mic, R. (2007). Orbital microwave measurement of river discharge and ice status. *Water Resources Research, 43*(4), W04405.

Brakenridge, G. R., Cohen, S., Kettner, A. J., De Groeve, T., Nghiem, S. V., Syvitski, J. P. M., & Fekete, B. M. (2012). Calibration of satellite measurements of river discharge using a global hydrology model. *Journal of Hydrology, 475*, 123–136.

Calmant, S., & Seyler, F. (2006). Continental surface waters from satellite altimetry. *Comptes Rendus Geoscience, 338*(14–15), 1113–1122.

Crétaux, J. F., et al. (2011). SOLS: A lake database to monitor in the Near Real Time water level and storage variations from remote sensing data. *Advances in Space Research, 47*(9), 1497–1507.

Dai, A., & Trenberth, K. E. (2002). Estimates of freshwater discharge from continents: Latitudinal and seasonal variations. *Journal of Hydrometeorology, 3*(6), 660–687.

Dai, A., Qian, T., Trenberth, K. E., & Milliman, J. D. (2009). Changes in continental freshwater discharge from 1948 to 2004. *Journal of Climate, 22*(10), 2773–2792.

Friedl, M. A., Sulla-Menashe, D., Tan, B., Schneider, A., Ramankutty, N., Sibley, A., & Huang, X. (2010). MODIS collection 5 global land cover: Algorithm refinements and characterization of new datasets. *Remote Sensing of Environment, 114*(1), 168–182.

Gleason, C. J., & Smith, L. C. (2014). Toward global mapping of river discharge using satellite images and at-many-stations hydraulic geometry. *Proceedings of the National Academy of Sciences, 111*(13), 4788–4791.

Gleason, C. J., Smith, L. C., & Lee, J. (2014). Retrieval of river discharge solely from satellite imagery and at-many-stations hydraulic geometry: Sensitivity to river form and optimization parameters. *Water Resources Research, 50*(12), 9604–9619.

GRDC (2014). In GRDC (Ed.), *River discharge data* (56068 Koblenz).

Grünler, S., Romeiser, R., & Stammer, D. (2013). Estimation of tidally influenced estuarine river discharge from space using along-track InSAR technology: A model-based feasibility study. *Journal of Geophysical Research: Oceans, 118*(7), 3679–3693.

Herschy, R. W. (2002). The uncertainty in a current meter measurement. *Flow Measurement and Instrumentation, 13*(5–6), 281–284.

Jarihani, A. A., Callow, J. N., McVicar, T. R., Van Niel, T. G., & Larsen, J. R. (2015a). Satellite-derived Digital Elevation Model (DEM) selection, preparation and correction for hydrodynamic modelling in large, low-gradient and data-sparse catchments. *Journal of Hydrology, 524*, 489–506.

Jarihani, A. A., Larsen, J. R., Callow, J. N., McVicar, T. R., & Johansen, K. (2015b). Where does all the water go? Partitioning water transmission losses in a data-sparse, multi-channel and low-gradient dryland river system using modelling and remote sensing. *Journal of Hydrology, 529*(Part 3), 1511–1529.

Jarihani, A. A., Callow, J. N., Johansen, K., & Gouweleeuw, B. (2013). Evaluation of multiple satellite altimetry data for studying inland water bodies and river floods. *Journal of Hydrology, 505*, 78–90.

Koblinsky, C. J., Clarke, R. T., Brenner, A. C., & Frey, H. (1993). Measurement of river level variations with satellite altimetry. *Water Resources Research, 29*(6), 1839–1848.

Kouraev, A. V., Zakharova, E. A., Samain, O., Mognard, N. M., & Cazenave, A. (2004). Ob' river discharge from TOPEX/Poseidon satellite altimetry (1992–2002). *Remote Sensing of Environment, 93*(1–2), 238–245.

LeFavour, G., & Alsdorf, D. (2005). Water slope and discharge in the Amazon River estimated using the shuttle radar topography mission digital elevation model. *Geophysical Research Letters, 32*(17), L17404.

Leon, J. G., Calmant, S., Seyler, F., Bonnet, M. P., Cauhopé, M., Frappart, F., ... Fraizy, P. (2006). Rating curves and estimation of average water depth at the upper Negro River based on satellite altimeter data and modeled discharges. *Journal of Hydrology, 328*(3–4), 481–496.

Leonard, J., Mietton, M., Najib, H., & Gourbesville, P. (2000). Rating curve modelling with Manning's equation to manage instability and improve extrapolation. *Hydrological Sciences Journal, 45*(5), 739–750.

Leopold, Luna B., & Maddock, Thomas, Jr. (1953). The hydraulic geometry of stream channels and some physiographic implications. *Geological Survey Professional Paper, 252* (57 pp.).

Manning, R. (1889). On the flow of water in open channels and pipes. *Transactions of the Institution of Civil Engineers of Ireland, 20*, 161–207.

Mersel, M. K., Smith, L. C., Andreadis, K. M., & Durand, M. T. (2013). Estimation of river depth from remotely sensed hydraulic relationships. *Water Resources Research, 49*(6), 3165–3179.

Nash, J. E., & Sutcliffe, J. V. (1970). River flow forecasting through conceptual models part I — A discussion of principles. *Journal of Hydrology, 10*(3), 282–290.

Negrel, J., Kosuth, P., & Bercher, N. (2011). Estimating river discharge from earth observation measurements of river surface hydraulic variables. *Hydrology and Earth System Sciences, 15*(6), 2049–2058.

Papa, F., Bala, S. K., Pandey, R. K., Durand, F., Gopalakrishna, V. V., Rahman, A., & Rossow, W. B. (2012). Ganga–Brahmaputra river discharge from Jason-2 radar altimetry: An update to the long-term satellite-derived estimates of continental freshwater forcing flux into the Bay of Bengal. *Journal of Geophysical Research: Oceans, 117*(C11), C11021.

Papa, F., Legresy, B., Mognard, N. M., Josberger, E. G., & Remy, F. (2002). Estimating terrestrial snow depth with the TOPEX-Poseidon altimeter and radiometer. *IEEE Transactions on Geoscience and Remote Sensing, 40*(10), 2162–2169.

Pavelsky, T., & Durand, M. (2012). Developing new algorithms for estimating river discharge from space. *Eos, Transactions American Geophysical Union, 93*(45), 457-457.

Pavelsky, T. M. (2014). Using width-based rating curves from spatially discontinuous satellite imagery to monitor river discharge. *Hydrological Processes, 28*(6), 3035–3040.

Pelletier, P. M. (1988). Uncertainties in the single determination of river discharge: A literature review. *Canadian Journal of Civil Engineering, 15*(5), 834–850.

Peña-Arancibia, J. L., Zhang, Y., Pagendam, D. E., Viney, N. R., Lerat, J., van Dijk, A. I. J. M., ... Frost, A. J. (2015). Streamflow rating uncertainty: Characterisation and impacts on model calibration and performance. *Environmental Modelling & Software, 63*, 32–44.

Plant, W. J., Keller, W. C., & Hayes, K. (2005). Measurement of river surface currents with coherent microwave systems. *IEEE Transactions on Geoscience and Remote Sensing, 43*(6), 1242–1257.

Rantz, S. E. (1982). Measurement and computation of streamflow. Measurement of stage and discharge. *US Geological Survey Water Supply Paper, 1*, 284.

Santos da Silva, J., Calmant, S., Seyler, F., Rotunno Filho, O. C., Cochonneau, G., & Mansur, W. J. (2010). Water levels in the Amazon basin derived from the ERS 2 and ENVISAT radar altimetry missions. *Remote Sensing of Environment, 114*(10), 2160–2181.

Schwatke, C., Dettmering, D., Bosch, W., & Seitz, F. (2015). DAHITI — An innovative approach for estimating water level time series over inland waters using multimission satellite altimetry. *Hydrology and Earth System Sciences, 19*(10), 4345–4364.

Shum, C. K., Ries, J. C., & Tapley, B. D. (1995). The accuracy and applications of satellite altimetry. *Geophysical Journal International, 121*(2), 321–336.

Smith, L. C., & Pavelsky, T. M. (2008). Estimation of river discharge, propagation speed, and hydraulic geometry from space: Lena River, Siberia. *Water Resources Research, 44*(3) (n/a-n/a).

Smith, L. C., Isacks, B. L., Bloom, A. L., & Murray, A. B. (1996). Estimation of discharge from three braided rivers using synthetic aperture radar satellite imagery: Potential application to ungaged basins. *Water Resources Research, 32*(7), 2021–2034.

Sneeuw, N., Lorenz, C., Devaraju, B., Tourian, M., Riegger, J., Kunstmann, H., & Bárdossy, A. (2014). Estimating runoff using hydro-geodetic approaches. *Surveys in Geophysics, 35*(6), 1333–1359.

Sulistioadi, Y. B., Tseng, K. H., Shum, C. K., Hidayat, H., Sumaryono, M., Suhardiman, A., ... Sunarso, S. (2015). Satellite radar altimetry for monitoring small rivers and lakes in Indonesia. *Hydrology and Earth System Sciences, 19*(1), 341–359.

Sun, W. C., Ishidaira, H., & Bastola, S. (2010). Towards improving river discharge estimation in ungauged basins: Calibration of rainfall-runoff models based on satellite observations of river flow width at basin outlet. *Hydrology and Earth System Sciences, 14*(10), 2011–2022.

Sun, W., Ishidaira, H., & Bastola, S. (2012a). Prospects for calibrating rainfall-runoff models using satellite observations of river hydraulic variables as surrogates for in situ river discharge measurements. *Hydrological Processes, 26*(6), 872–882.

Sun, W., Ishidaira, H., & Bastola, S. (2012b). Calibration of hydrological models in ungauged basins based on satellite radar altimetry observations of river water level. *Hydrological Processes, 26*(23), 3524–3537.

Tang, Q., Gao, H., Lu, H., & Lettenmaier, D. P. (2009). Remote sensing: Hydrology. *Progress in Physical Geography, 33*(4), 490–509.

Tarpanelli, A., Barbetta, S., Brocca, L., & Moramarco, T. (2013). River discharge estimation by using altimetry data and simplified flood routing modeling. *Remote Sensing, 5*(9), 4145.

Temimi, M., Lacava, T., Lakhankar, T., Tramutoli, V., Ghedira, H., Ata, R., & Khanbilvardi, R. (2011). A multi-temporal analysis of AMSR-E data for flood and discharge monitoring during the 2008 flood in Iowa. *Hydrological Processes, 25*(16), 2623–2634.

Tomkins, K. M. (2014). Uncertainty in streamflow rating curves: Methods, controls and consequences. *Hydrological Processes, 28*(3), 464–481.

Tourian, M. J., Sneeuw, N., & Bárdossy, A. (2013). A quantile function approach to discharge estimation from satellite altimetry (ENVISAT). *Water Resources Research, 49*(7), 4174–4186.

Vörösmarty, C., et al. (2001). Global water data: A newly endangered species. *Eos, Transactions American Geophysical Union, 82*(5), 54–58.

Zelli, C., & Aerospazio, A. (1999). ENVISAT RA-2 advanced radar altimeter: Instrument design and pre-launch performance assessment review. *Acta Astronautica, 44*(7–12), 323–333.